

Complexity of Quantum-Mechanical Evolutions from Probability Amplitudes

Carlo Cafaro^{1,2}, Leonardo Rossetti^{3,1}, Paul M. Alsing¹

¹*University at Albany-SUNY, Albany, NY 12222, USA*

²*SUNY Polytechnic Institute, Utica, NY 13502, USA and*

³*University of Camerino, I-62032 Camerino, Italy*

We study the complexity of both time-optimal and time sub-optimal quantum Hamiltonian evolutions connecting arbitrary source and a target states on the Bloch sphere equipped with the Fubini-Study metric. This investigation is performed in a number of steps. First, we describe each unitary Schrödinger quantum evolution by means of the path length, the geodesic efficiency, the speed efficiency, and the curvature coefficient of its corresponding dynamical trajectory linking the source state to the target state. Second, starting from a classical probabilistic setting where the so-called information geometric complexity can be employed to describe the complexity of entropic motion on curved statistical manifolds underlying the physics of systems when only partial knowledge about them is available, we transition into a deterministic quantum setting. In this context, after proposing a definition of the complexity of a quantum evolution, we present a notion of quantum complexity length scale. In particular, we discuss the physical significance of both quantities in terms of the accessed (i.e., partial) and accessible (i.e., total) parametric volumes of the regions on the Bloch sphere that specify the quantum mechanical evolution from the source to the target states. Third, after calculating the complexity measure and the complexity length scale for each one of the two quantum evolutions, we compare the behavior of our measures with that of the path length, the geodesic efficiency, the speed efficiency, and the curvature coefficient. We find that, in general, efficient quantum evolutions are less complex than inefficient evolutions. However, we also observe that complexity is more than length. Indeed, longer paths that are sufficiently bent can exhibit a behavior that is less complex than that of shorter paths with a smaller curvature coefficient.

PACS numbers: Complexity (89.70.Eg), Entropy (89.70.Cf), Probability Theory (02.50.Cw), Quantum Computation (03.67.Lx), Quantum Information (03.67.Ac), Riemannian Geometry (02.40.Ky).

I. INTRODUCTION

Quantum complexity in theoretical physics is a highly interesting quantity. For example, regarding black holes as holographically described by a collection of qubits that evolve under Hamiltonians that exhibit fingerprints of maximal quantum chaos, complexity can be used to specify the phenomena of particle growth and information spreading near black hole horizons [1]. In this context, the so-called holographic complexity (i.e., the complexity of a holographic quantum state) is related to the growth of the volume in the bulk geometry beyond the event horizon in black holes [2–5]. In many-body physics, complexity can be used to distinguish highly entangled quantum states of condensed matter systems and to characterize thermalization and transport in quantum many-body systems [6–9]. The usefulness of complexity, in this context, emerges once the link between quantum chaos and complexity in chaotic quantum systems is made transparent [8–10].

There are several notions of complexity in quantum physics. For instance, one can speak of the complexity of a quantum state (state complexity, [11, 12]), the complexity of a quantum circuit (circuit complexity, [13, 14]) or, alternatively, the complexity of an operator (operator complexity, [15–18]). Despite their differences, like most measures of complexity, each one of these measures captures the essential idea that the complexity of a composite object scales like the number of elementary elements needed to construct it [19–21]. Depending on the specific context, the scaling with the number of elementary elements can be conveniently expressed in terms of geometrically intuitive concepts like lengths and volumes. In the context of theoretical computer science, Kolmogorov suggested in Ref. [22] that the complexity of a sequence can be expressed as the length of the shortest Turing machine program that generates it. In information theory, Rissanen proposed in Refs. [23, 24] that the minimal code length of an ensemble of messages, averaged over the ensemble, specifies the complexity of an ensemble of messages in information theory.

The relevance of the concepts of length and volumes is essential in the characterization of complexity in a quantum mechanical setting as well. For example, the state complexity is the complexity of a quantum state described in terms of the smallest local unitary circuit that can generate the state from an initial simple (i.e., factorizable) reference quantum state. Interestingly, a geometric formulation of the state complexity was first proposed while investigating the complexity of quantum states in continuous many-body systems. Specifically, the state complexity of a target state generated by acting on a source state with a set of parametrized unitary operators was expressed as the length of the shortest path measured with the Fubini-Study metric and associated with an allowed realization of the unitary operator [11]. Moreover, quantum circuits are made of quantum gates that act on quantum states. In particular, the

circuit complexity specifies the number of primitive gates in the smallest circuit that implement a transformation that acts on a given quantum state [13, 14]. It is discrete in nature and, in addition, is a natural complexity measure for scientists trying to actually build quantum circuits out of component gates. Interestingly, the definitions of state and circuit complexities are not unrelated since the state complexity is the complexity of the least complex unitary operator that connects source and the target states. The geometric characterization of the concept of circuit complexity was proposed by Nielsen and collaborators in Refs. [25–27]. In this geometric formulation, the circuit complexity of a unitary operator U is continuous in nature and is equal to the length of the minimal geodesic on the unitary group that joins the identity operator to U . The length of these geodesic curves, in turn, provide a lower bound for the minimum number of quantum gates needed to generate the unitary operator U . Finally, operator complexity describes the temporal growth of the size of an operator under the Heisenberg or Lindblad time evolutions for closed and open quantum systems, respectively. When evaluated with respect to the so-called Krylov basis, the operator complexity is called Krylov complexity [15]. For a presentation of useful techniques to handle Nielsen’s complexity of nontrivial dynamical systems, we refer to Refs. [28, 29]. Furthermore, for a description of a rather surprising connection between Krylov’s and Nielsen’s complexities, we suggest Ref. [30]. In Ref. [18], while studying the temporal change of the displacement operator during the unitary evolution of many-body quantum systems governed by symmetries, the expectation value of the Krylov complexity operator was shown to be equal to the volume of the corresponding classical phase space. The link between Krylov complexity and volume was further discussed in the context of specific quantum field theoretic settings in Ref. [16]. In particular, the scaling of this complexity with the volume was justified by demonstrating that the Krylov complexity is equal to the average particle number. Then, applying the proportionality between the volume and the average particle number, the link was properly motivated.

In Ref. [31], we presented an information geometric theoretical approach to describe and, to a certain extent, comprehend the complex behavior of evolutions of quantum systems in pure and mixed states. The comparative analysis was probabilistic in nature, it employed a complexity measure that relied on a temporal averaging procedure along with a long-time limit, and was limited to analyzing expected geodesic evolutions on the underlying manifolds. In particular, we analyzed the complexity of geodesic paths on the manifolds of single-qubit pure and mixed quantum states equipped with the Fubini-Study metric [32] and the Sjöqvist [33] metric, respectively. We demonstrated in an analytical fashion that the evolution of mixed quantum states in the Bloch ball is more complex than the evolution of pure states on the Bloch sphere. We also confirmed that the ranking based on our proposed measure of complexity, a quantity that specifies the asymptotic temporal behavior of an averaged volume of the region explored on the manifold during the evolution of the systems, concurs with the ranking based on the geodesic length of the corresponding paths. Last but not least, we found that the complexity of the Bures manifold was softened compared to the Sjöqvist manifold when we focused on geodesic lengths and curvature properties [34].

In this paper, going beyond the work of Ref. [31] and given the fundamental role played by the concepts of length and volume in the characterization of the complexity of quantum processes, the goal is to provide a clear comparative analysis of the complexity of quantum evolutions, both geodesic and nongeodesic, on the Bloch sphere for two-level quantum systems. In particular, to enhance our comprehension of the physical significance of the newly proposed concept of complexity, the comparative analysis is carried out also in terms of additional quantifiers with an established physical meaning. The list of these additional measure includes path lengths, geodesic and speed efficiencies and, finally, curvature coefficients of the quantum evolutions.

To the best of our knowledge, we aim to tackle a range of unexplored questions in the literature, some examples of which include:

- [i] Does the complexity of a quantum evolution from an initial to a final state under a given Hamiltonian encode information beyond the one encoded in the concept of length of the quantum evolution path?
- [ii] Are complex quantum evolutions necessarily characterized by a large amount of wasted energy?
- [iii] Are quantum evolutions characterized by longer paths necessarily more complex than the ones specified by shorter paths connecting the same initial and final quantum states?
- [iv] Is time-optimality a synonymous with reduced complexity?
- [v] Can quantum evolutions that occur at lower quantum speeds and with larger waste of energy resources be less complex than very fast evolutions that happen with negligible amounts of wasted energy?

The rest of the paper is organized as follows. In Section II, we introduce optimal and sub-optimal quantum Hamiltonian evolutions connecting arbitrary source (i.e., initial) and a target (i.e., final) states on the Bloch sphere equipped with the Fubini-Study metric. In particular, we characterize both evolutions in terms of the concepts of path length [35–37], geodesic efficiency [38, 39], speed efficiency [40], and curvature coefficients [41, 42] of the dynamical trajectories that connect the given initial and final states. In Section III, we begin by considering a

classical probabilistic setting where the so-called information geometric complexity is generally used to characterize the complexity of entropic motion on curved statistical manifolds underlying the physics of systems when only limited information about them is available [43–46]. Then, moving to a deterministic quantum setting, we present our definition of complexity of a quantum evolution along with a notion of quantum complexity length scale. We explicitly discuss the physical meaning of both concepts and, in particular, we discuss the fact that we express both concepts in terms of accessed and accessible parametric volumes of the regions on the Bloch sphere that specify the evolution from the source to the target states. In Section IV, we calculate the complexity measure and the complexity length scale of each one of the two (families of) quantum evolutions mentioned in Section II. In particular, for each quantum evolution, we compare the complexity measure and the complexity length scale with the path length, the geodesic efficiency, the speed efficiency, and the curvature coefficient. In Section V, we locate our summary of results and final remarks. Finally, we place technical details in Appendix A and Appendix B.

II. HAMILTONIAN EVOLUTIONS

In this section, we present optimal and sub-optimal quantum Hamiltonian evolutions linking arbitrary source and target states on the Bloch sphere. Specifically, we study both evolutions by means of the notions of path length [35–37], geodesic efficiency [38, 39], speed efficiency [40], and curvature coefficients [41, 42] of the dynamical trajectories that join the given initial and final states.

A. Geodesic evolution

The quantum evolution that specifies a geodesic evolution on the Bloch sphere by evolving the initial state $|A\rangle \stackrel{\text{def}}{=} |\psi(t_A)\rangle$ into the final state $|B\rangle \stackrel{\text{def}}{=} |\psi(t_B)\rangle$ in a time interval $t_{AB} \stackrel{\text{def}}{=} t_B - t_A$ is defined by the stationary Hamiltonian [37, 47–53]

$$\mathbf{H}_{\text{opt}} \stackrel{\text{def}}{=} \mathbf{h}_{\text{opt}} \cdot \boldsymbol{\sigma} = E \frac{\hat{a} \times \hat{b}}{\sqrt{(\hat{a} \times \hat{b}) \cdot (\hat{a} \times \hat{b})}} \cdot \boldsymbol{\sigma}, \quad (1)$$

with $\boldsymbol{\sigma} \stackrel{\text{def}}{=} (\sigma_x, \sigma_y, \sigma_z)$ being the vector operator of Pauli matrices. We assume here to have $0 \leq \theta_{AB} \leq \pi$ with $\sqrt{(\hat{a} \times \hat{b}) \cdot (\hat{a} \times \hat{b})} = \sin(\theta_{AB})$. The quantity E denotes energy, while the components of the vector \mathbf{h}_{opt} are measured in energy units. However, we loosely denote \mathbf{h}_{opt} as the “magnetic” field vector. The unit vectors \hat{a} and \hat{b} are the Bloch vectors that correspond to the states $|A\rangle$ and $|B\rangle$, respectively, with $\rho_A \stackrel{\text{def}}{=} (\mathbf{1} + \hat{a} \cdot \boldsymbol{\sigma})/2$ and $\rho_B \stackrel{\text{def}}{=} (\mathbf{1} + \hat{b} \cdot \boldsymbol{\sigma})/2$. Clearly, “ $\mathbf{1}$ ” represents the identity operator here. The unitary evolution operator $U_{\text{opt}}(t)$ that corresponds to \mathbf{H}_{opt} in Eq. (1) is given by

$$U_{\text{opt}}(t) \stackrel{\text{def}}{=} \exp\left[-\frac{i}{\hbar} \mathbf{H}_{\text{opt}} t\right] = \cos\left(\frac{E}{\hbar} t\right) \mathbf{1} - i \sin\left(\frac{E}{\hbar} t\right) \frac{\hat{a} \times \hat{b}}{\sin(\theta_{AB})} \cdot \boldsymbol{\sigma}, \quad (2)$$

with $|\psi(t)\rangle \stackrel{\text{def}}{=} U_{\text{opt}}(t, t_A) |A\rangle = e^{-\frac{i}{\hbar} \mathbf{H}_{\text{opt}}(t-t_A)} |A\rangle$ for any $t_A \leq t \leq t_B$. The unitary time propagator defined by $U_{\text{opt}}(t)$ in Eq. (2) brings $|A\rangle$ into $|B\rangle$ in a minimum time interval given by $t_{AB}^{\text{opt}} \stackrel{\text{def}}{=} \hbar \theta_{AB} / (2E)$, along a path of (shortest) length equal to θ_{AB} . In terms of the geodesic efficiency $\eta_{\text{GE}} \stackrel{\text{def}}{=} s_0/s$ of the quantum evolution [38, 39],

$$\eta_{\text{GE}} \stackrel{\text{def}}{=} \frac{s_0}{s} = \frac{2 \arccos[|\langle A|B\rangle|]}{\int_{t_A}^{t_B} \frac{2}{\hbar} \Delta E(t) dt}, \quad (3)$$

we have that $s_0 = \theta_{AB}$, $t_B - t_A = t_{AB}^{\text{opt}} \stackrel{\text{def}}{=} \hbar \theta_{AB} / (2E)$, $\Delta E^2 \stackrel{\text{def}}{=} \langle A | \mathbf{H}_{\text{opt}}^2 | A \rangle - \langle A | \mathbf{H}_{\text{opt}} | A \rangle^2 = E^2$, and, therefore, $s = \theta_{AB}$. Thus, $\eta_{\text{GE}}^{\text{opt}} = 1$ and the evolution is geodesic. Notice that s_0 denotes the distance along the shortest geodesic path that joins $|A\rangle$ and $|B\rangle$ on the complex projective Hilbert space. The quantity s , instead, defines the distance along the actual dynamical trajectory $\gamma(t) : t \mapsto |\psi(t)\rangle$ that corresponds to the evolution under \mathbf{H}_{opt} of the state vector $|\psi(t)\rangle$, with $t_A \leq t \leq t_B$. The evolution specified by $U_{\text{opt}}(t)$ in Eq. (2) occurs also without any waste of energy

resources since its speed efficiency [40],

$$\eta_{\text{SE}} \stackrel{\text{def}}{=} \frac{\Delta H_\rho}{\|\mathbf{H}\|_{\text{SP}}} = \frac{\sqrt{\text{tr}(\rho \mathbf{H}^2) - [\text{tr}(\rho \mathbf{H})]^2}}{\max[\sqrt{\text{eig}(\mathbf{H}^\dagger \mathbf{H})}]}, \quad (4)$$

equals to one. This is a consequence of the fact that the energy uncertainty ΔH_ρ , where $\rho = \rho(t) \stackrel{\text{def}}{=} [\mathbf{1} + \hat{\mathbf{a}}(t) \cdot \boldsymbol{\sigma}] / 2$ and $t_A \leq t \leq t_B$ equals the spectral norm $\|\mathbf{H}\|_{\text{SP}}$ of the Hamiltonian \mathbf{H}_{opt} in Eq. (1). Specifically, from Eqs. (1) and (4), we get

$$\eta_{\text{SE}}^{\text{opt}} = \eta_{\text{SE}}^{\text{opt}}(t) \stackrel{\text{def}}{=} \frac{\sqrt{\mathbf{h}_{\text{opt}}^2 - (\hat{\mathbf{a}} \cdot \mathbf{h}_{\text{opt}})^2}}{\sqrt{\mathbf{h}_{\text{opt}}^2}} = 1, \quad (5)$$

since $\hat{\mathbf{a}} \cdot \mathbf{h}_{\text{opt}} = 0$ for any instant $t \in [t_A, t_B]$. Therefore, a trajectory is wasteful in energy (speed) whenever the magnetic field has a component along the Bloch vector, thus generating useless rotations about $\hat{\mathbf{a}}$. Finally, if we consider a quantum evolution specified by a traceless Hamiltonian $\mathbf{H} \stackrel{\text{def}}{=} \mathbf{h} \cdot \boldsymbol{\sigma}$, with corresponding curvature coefficient given by [41, 42]

$$\kappa_{\text{AC}}^2(\hat{\mathbf{a}}, \mathbf{h}) \stackrel{\text{def}}{=} 4 \frac{(\hat{\mathbf{a}} \cdot \mathbf{h})^2}{\mathbf{h}^2 - (\hat{\mathbf{a}} \cdot \mathbf{h})^2}, \quad (6)$$

we have

$$\kappa_{\text{AC}}^2(\hat{\mathbf{a}}, \mathbf{h}_{\text{opt}}) = 0, \quad (7)$$

since \mathbf{h}_{opt} is constantly orthogonal to $\hat{\mathbf{a}}$. Given the fact that $\kappa_{\text{AC}}^2(\hat{\mathbf{a}}, \mathbf{h})$ in Eq. (6) is a measure of the bending of the path on the Bloch sphere, a path with zero curvature exhibits no bending at all. For more details on the concept of curvature for both stationary and nonstationary Hamiltonian evolutions, we suggest Refs. [41, 42]. In summary, the evolution specified by Eq. (2) occurs with unit geodesic efficiency (i.e., with the shortest path length, that is, $\eta_{\text{GE}}^{\text{opt}} = 1$), with unit speed efficiency (i.e., with no waste of energy along the path, that is, $\eta_{\text{SE}}^{\text{opt}}(t)$ for any $t \in [t_A, t_B]$) and, finally, with zero curvature coefficient (i.e., with no bending of the path, that is $(\kappa_{\text{AC}}^2)_{\text{opt}} \stackrel{\text{def}}{=} \kappa_{\text{AC}}^2(\hat{\mathbf{a}}, \mathbf{h}_{\text{opt}}) = 0$).

B. Nongeodesic evolution

The quantum evolution that describes a nongeodesic evolution on the Bloch sphere by evolving the initial state $|A\rangle \stackrel{\text{def}}{=} |\psi(t_A)\rangle$ into the final state $|B\rangle \stackrel{\text{def}}{=} |\psi(t_B)\rangle$ in a time interval $t_{AB} \stackrel{\text{def}}{=} t_B - t_A$ is specified by the stationary Hamiltonian [53]

$$\mathbf{H}_{\text{sub-opt}} \stackrel{\text{def}}{=} \mathbf{h}_{\text{sub-opt}} \cdot \boldsymbol{\sigma} = E \left[\cos(\alpha) \frac{\hat{\mathbf{a}} + \hat{\mathbf{b}}}{\sqrt{(\hat{\mathbf{a}} + \hat{\mathbf{b}}) \cdot (\hat{\mathbf{a}} + \hat{\mathbf{b}})}} + \sin(\alpha) \frac{\hat{\mathbf{a}} \times \hat{\mathbf{b}}}{\sqrt{(\hat{\mathbf{a}} \times \hat{\mathbf{b}}) \cdot (\hat{\mathbf{a}} \times \hat{\mathbf{b}})}} \right] \cdot \boldsymbol{\sigma}, \quad (8)$$

with $0 \leq \alpha \leq \pi$. Assuming to have $0 \leq \theta_{AB} \leq \pi$, $\sqrt{(\hat{\mathbf{a}} \times \hat{\mathbf{b}}) \cdot (\hat{\mathbf{a}} \times \hat{\mathbf{b}})} = \sin(\theta_{AB})$ and $\sqrt{(\hat{\mathbf{a}} + \hat{\mathbf{b}}) \cdot (\hat{\mathbf{a}} + \hat{\mathbf{b}})} = 2 \cos(\theta_{AB}/2)$. Therefore, the Hamiltonian in Eq. (8) can be recast as

$$\mathbf{H}_{\text{sub-opt}} = E \left[\cos(\alpha) \frac{\hat{\mathbf{a}} + \hat{\mathbf{b}}}{2 \cos(\frac{\theta_{AB}}{2})} + \sin(\alpha) \frac{\hat{\mathbf{a}} \times \hat{\mathbf{b}}}{\sin(\theta_{AB})} \right] \cdot \boldsymbol{\sigma}. \quad (9)$$

For a schematic depiction of the unit vectors $\hat{\mathbf{n}}_{\text{opt}} \stackrel{\text{def}}{=} \mathbf{h}_{\text{sub}} / \sqrt{\mathbf{h}_{\text{sub}} \cdot \mathbf{h}_{\text{sub}}}$ and $\hat{\mathbf{n}}_{\text{sub-opt}} \stackrel{\text{def}}{=} \mathbf{h}_{\text{sub-opt}} / \sqrt{\mathbf{h}_{\text{sub-opt}} \cdot \mathbf{h}_{\text{sub-opt}}}$ that specify the optimal and sub-optimal Hamiltonians in Eqs. (1) and (8), respectively, we refer to Fig. 1. In analogy to what we mentioned in the optimal scenario case, the unit vectors $\hat{\mathbf{a}}$ and $\hat{\mathbf{b}}$ denote the Bloch vectors that correspond to the states $|A\rangle$ and $|B\rangle$, respectively, with $\rho_A \stackrel{\text{def}}{=} (\mathbf{1} + \hat{\mathbf{a}} \cdot \boldsymbol{\sigma}) / 2$ and $\rho_B \stackrel{\text{def}}{=} (\mathbf{1} + \hat{\mathbf{b}} \cdot \boldsymbol{\sigma}) / 2$. The unitary evolution operator $U_{\text{sub-opt}}(t)$ that corresponds to $\mathbf{H}_{\text{sub-opt}}$ in Eq. (8) is given by

$$U_{\text{sub-opt}}(t) \stackrel{\text{def}}{=} \exp \left[-\frac{i}{\hbar} \mathbf{H}_{\text{sub-opt}} t \right] = \cos \left(\frac{E}{\hbar} t \right) \mathbf{1} - i \sin \left(\frac{E}{\hbar} t \right) \left[\cos(\alpha) \frac{\hat{\mathbf{a}} + \hat{\mathbf{b}}}{2 \cos(\frac{\theta_{AB}}{2})} + \sin(\alpha) \frac{\hat{\mathbf{a}} \times \hat{\mathbf{b}}}{\sin(\theta_{AB})} \right] \cdot \boldsymbol{\sigma}, \quad (10)$$

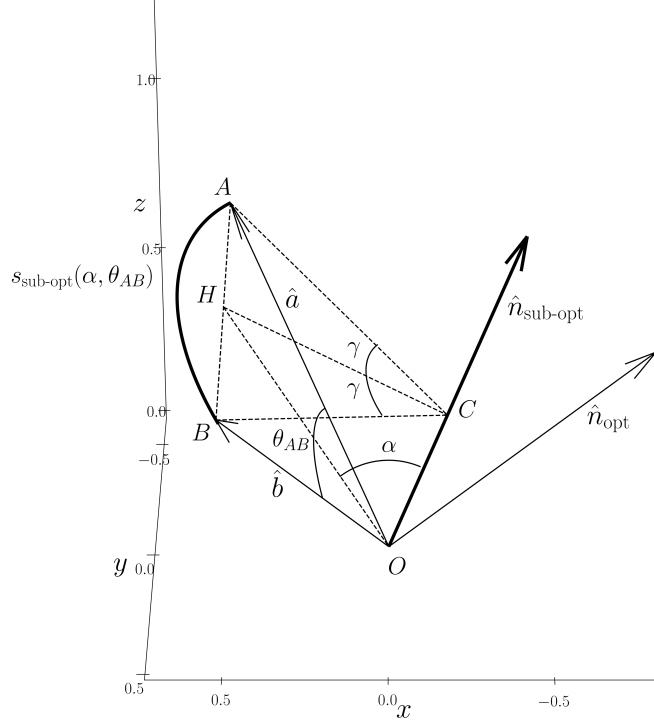


FIG. 1: Illustration of the unit vectors $\hat{n}_{\text{opt}} \stackrel{\text{def}}{=} (\hat{a} \times \hat{b}) / \|\hat{a} \times \hat{b}\|$ and $\hat{n}_{\text{sub-opt}} \stackrel{\text{def}}{=}} \cos(\alpha) \left[(\hat{a} + \hat{b}) / \|\hat{a} + \hat{b}\| \right] + \sin(\alpha) \left[(\hat{a} \times \hat{b}) / \|\hat{a} \times \hat{b}\| \right]$ characterizing the optimal (thin black) and sub-optimal (thick black) rotation axes, respectively. The initial and final unit Bloch vectors \hat{a} and \hat{b} , respectively, satisfy the condition $\hat{a} \cdot \hat{b} = \cos(\theta_{AB})$. The sub-optimal unitary evolution that defines the transition from \hat{a} to \hat{b} is characterized by $\hat{n}_{\text{sub-opt}}$ and the rotation angle $\phi \stackrel{\text{def}}{=} 2\gamma$. Finally, the length of the nongeodesic path that connects these two Bloch vectors via the sub-optimal unitary evolution is equal to $s_{\text{sub-opt}}(\alpha, \theta_{AB}) \stackrel{\text{def}}{=} \overline{AC}(\alpha, \theta_{AB}) \phi(\alpha, \theta_{AB})$ (thick black).

with $|\psi(t)\rangle \stackrel{\text{def}}{=} U_{\text{sub-opt}}(t, t_A) |A\rangle = e^{-\frac{i}{\hbar} H_{\text{sub-opt}}(t-t_A)} |A\rangle$ for any $t_A \leq t \leq t_B$. The unitary time propagator defined by $U_{\text{sub-opt}}(t)$ in Eq. (2) brings $|A\rangle$ into $|B\rangle$ in a sub-optimal time interval given by $t_{AB}(\alpha) = t_{AB}^{\text{sub-opt}}(\alpha)$ along a path of length $s(\alpha)$. The quantities $t_{AB}(\alpha)$ and $s(\alpha)$ are given by [53]

$$t_{AB}(\alpha) \stackrel{\text{def}}{=} \frac{\hbar}{E} \arccos \left[\sin(\alpha) \frac{\cos(\frac{\theta_{AB}}{2})}{\sqrt{1 - \cos^2(\alpha) \cos^2(\frac{\theta_{AB}}{2})}} \right], \quad (11)$$

and

$$s(\alpha) \stackrel{\text{def}}{=} 2\sqrt{1 - \cos^2(\alpha) \cos^2(\frac{\theta_{AB}}{2})} \arccos \left[\sin(\alpha) \frac{\cos(\frac{\theta_{AB}}{2})}{\sqrt{1 - \cos^2(\alpha) \cos^2(\frac{\theta_{AB}}{2})}} \right], \quad (12)$$

respectively. Since $s(\alpha) \geq s_0 = \theta_{AB}$, the geodesic efficiency η_{GE} in Eq. (3) is less than one in this sub-optimal case. Specifically, from Eqs. (3) and (12), we get

$$(\eta_{\text{GE}})_{\text{sub-opt}}(\alpha) = \frac{\theta_{AB}}{2\sqrt{1 - \cos^2(\alpha) \cos^2(\frac{\theta_{AB}}{2})} \arccos \left[\sin(\alpha) \frac{\cos(\frac{\theta_{AB}}{2})}{\sqrt{1 - \cos^2(\alpha) \cos^2(\frac{\theta_{AB}}{2})}} \right]}. \quad (13)$$

Furthermore, the evolution specified by $U_{\text{sub-opt}}(t)$ in Eq. (2) happens with some waste of energy resources since its speed efficiency in Eq. (4) is less than one in this sub-optimal scenario. Indeed, decomposing \mathbf{h} as $\mathbf{h} = \mathbf{h}_{\parallel} + \mathbf{h}_{\perp} = (\mathbf{h} \cdot \hat{a}) \hat{a} + [\mathbf{h} - (\mathbf{h} \cdot \hat{a}) \hat{a}]$, for $\mathbf{h} = \mathbf{h}_{\text{sub-opt}}$, we get $\mathbf{h}_{\parallel}^2 = E^2 \cos^2(\alpha) \cos^2(\theta_{AB}/2)$ and $\mathbf{h}_{\perp}^2 =$

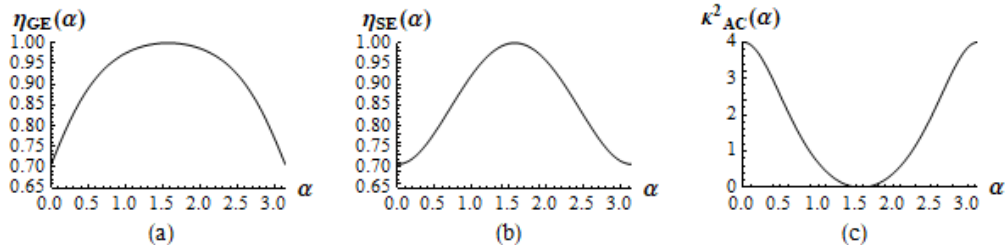


FIG. 2: Plots of the geodesic efficiency $\eta_{\text{GE}}(\alpha)$, the speed efficiency $\eta_{\text{SE}}(\alpha)$, and the curvature coefficient $\kappa_{\text{AC}}^2(\alpha)$ versus $\alpha \in [0, \pi]$ in (a), (b), and (c), respectively. Note that for $\alpha = \pi/2 \simeq 1.57$, $\eta_{\text{GE}} = 1$, $\eta_{\text{SE}} = 1$, and $\kappa_{\text{AC}}^2 = 0$.

$E^2 [1 - \cos^2(\alpha) \cos^2(\theta_{AB}/2)]$. Then, noting that the speed efficiency of (traceless) stationary quantum evolutions can be recast as $\eta_{\text{SE}} = \sqrt{\mathbf{h}_{\perp}^2 / (\mathbf{h}_{\perp}^2 + \mathbf{h}_{\parallel}^2)}$, we have

$$(\eta_{\text{SE}})_{\text{sub-opt}}(\alpha) = \sqrt{1 - \cos^2(\alpha) \cos^2\left(\frac{\theta_{AB}}{2}\right)}. \quad (14)$$

Unlike the optimal case, in the sub-optimal case $(\hat{a} \cdot \mathbf{h}_{\text{sub-opt}})^2 = \mathbf{h}_{\parallel}^2 \neq 0$. For this reason there is some waste of energy along the path and, as a consequence, the speed efficiency is not maximal (i.e., not equal to one). Finally, given that the curvature coefficient in Eq. (6) can be recast as $\kappa_{\text{AC}}^2 = 4(\mathbf{h}_{\parallel}^2 / \mathbf{h}_{\perp}^2)$, we obtain

$$(\kappa_{\text{AC}}^2)_{\text{sub-opt}}(\alpha) = 4 \frac{\cos^2(\alpha) \cos^2\left(\frac{\theta_{AB}}{2}\right)}{1 - \cos^2(\alpha) \cos^2\left(\frac{\theta_{AB}}{2}\right)}. \quad (15)$$

In Fig. 2, we plot the geodesic efficiency, the speed efficiency, and the curvature coefficient in Eqs. (13), (14), and (15), respectively, versus $\alpha \in [0, \pi]$ for $\theta_{AB} = \pi/2$. Summing up, the quantum evolution defined in Eq. (10) happens with sub-unit geodesic efficiency (i.e., without the shortest path length, that is, $(\eta_{\text{GE}})_{\text{sub-opt}}$ in Eq. (13) is strictly less than one), with sub-unit speed efficiency (i.e., with some waste of energy along the path, that is, $(\eta_{\text{SE}})_{\text{sub-opt}}$ in Eq. (14) is strictly less than one) and, finally, with nonzero curvature coefficient (i.e., with some bending of the path, that is $(\kappa_{\text{AC}}^2)_{\text{sub-opt}} \stackrel{\text{def}}{=} \kappa_{\text{AC}}^2(\hat{a}, \mathbf{h}_{\text{sub-opt}})$ in Eq. (15) is strictly greater than zero).

Having presented several aspects of the Hamiltonian evolutions being considered in this paper, we are ready to introduce our proposed notions of complexity and complexity length scale in the next section.

III. COMPLEXITY

In this section, to better motivate the introduction of our proposed concepts of *complexity* and *complexity length scale* of a quantum evolution for a qubit state evolving under the action of an Hamiltonian that specifies a time-dependent Schrödinger equation, we briefly present our original measure of complexity of motion on curved manifolds of probability distributions in a probabilistic classical setting when only partial knowledge about the system under investigation is available.

A. Probabilistic classical setting

We begin by recalling the concepts of information geometric complexity (IGC) and information geometric entropy (IGE) [43, 44]. Before presenting formal definitions and more technical details, let us point out at the beginning that the IGC is basically the exponential of the IGE. The latter, in turn, represents the logarithm of the volume of the parametric region accessed by the system during its (maximally probable, from an entropic standpoint) geodesic evolution from an initial to a final point (i.e., a probability distribution) on the underlying curved statistical manifold.

The IGE is a measure of complexity that was originally presented in Ref. [43] in the framework of the so-called Information Geometric Approach to Chaos (IGAC) [44]. For a compact presentation of the IGAC, we suggest Refs. [54, 55].

In its original classical setting characterized by probability density functions, the IGE can be introduced as follows. Suppose that the points $\{p(x; \xi)\}$ of an N_c -dimensional curved statistical manifold \mathcal{M}_s are parametrized by N_c -real valued variables $(\xi^1, \dots, \xi^{N_c})$, with \mathcal{M}_s defined as

$$\mathcal{M}_s \stackrel{\text{def}}{=} \left\{ p(x; \xi) : \xi \stackrel{\text{def}}{=} (\xi^1, \dots, \xi^{N_c}) \in \mathcal{D}_\xi^{\text{tot}} \right\}. \quad (16)$$

Moreover, suppose that while the microvariables x that characterize the probability distributions $\{p(x; \xi)\}$ belong to the continuous microspace \mathcal{X} , the macrovariables ξ are elements of the parameter space $\mathcal{D}_\xi^{\text{tot}}$ given by

$$\mathcal{D}_\xi^{\text{tot}} \stackrel{\text{def}}{=} (\mathcal{I}_{\xi^1} \otimes \mathcal{I}_{\xi^2} \dots \otimes \mathcal{I}_{\xi^{N_c}}) \subseteq \mathbb{R}^{N_c}. \quad (17)$$

Observe that \mathcal{I}_{ξ^k} in Eq. (17) denotes a subset of \mathbb{R}^N and specifies the range of acceptable values for the statistical macrovariables ξ^k where $1 \leq k \leq N_c$. The IGE is a meaningful measure of temporal complexity of geodesic paths on \mathcal{M}_s in the IGAC context. It is formally defined as

$$\mathcal{S}_{\mathcal{M}_s}(\tau) \stackrel{\text{def}}{=} \log \widetilde{\text{vol}}[\mathcal{D}_\xi(\tau)], \quad (18)$$

where the average dynamical statistical volume $\widetilde{\text{vol}}[\mathcal{D}_\xi(\tau)]$ is given by

$$\widetilde{\text{vol}}[\mathcal{D}_\xi(\tau)] \stackrel{\text{def}}{=} \frac{1}{\tau} \int_0^\tau \text{vol}[\mathcal{D}_\xi(\tau')] d\tau'. \quad (19)$$

Since we take these volumes to be positive quantities, whenever we write $\text{vol}[\cdot]$, we really mean $|\text{vol}[\cdot]| \geq 0$. Furthermore, bear in mind that $\mathcal{D}_\xi(\tau')$ in Eq. (19) represents an N_c -dimensional subspace of $\mathcal{D}_\xi^{\text{tot}} \subseteq \mathbb{R}^{N_c}$ whose elements $\{\xi\}$ with $\xi \stackrel{\text{def}}{=} (\xi^1, \dots, \xi^{N_c})$ fulfill $\xi^k(\tau_0) \leq \xi^k \leq \xi^k(\tau_0 + \tau')$ where τ_0 is the initial value assumed by the affine parameter τ' that specifies the geodesics on \mathcal{M}_s as will be explained in more depth soon. The tilde symbol in Eq. (19) is employed to denote the temporal average operation. Furthermore, we remark that $\widetilde{\text{vol}}[\mathcal{D}_\xi(\tau)]$ in Eq. (19) is determined by two sequential integration procedures. The first integration is performed over the accessed parameter space $\mathcal{D}_\xi(\tau')$ and yields $\text{vol}[\mathcal{D}_\xi(\tau')]$. The second integration, instead, yields $\widetilde{\text{vol}}[\mathcal{D}_\xi(\tau)]$ and specifies a temporal averaging procedure performed over the duration τ of the geodesic evolution on the manifold \mathcal{M}_s . The quantity $\text{vol}[\mathcal{D}_\xi(\tau')]$ in the right-hand-side of Eq. (19) denotes the volume of an extended region on \mathcal{M}_s and is defined as,

$$\text{vol}[\mathcal{D}_\xi(\tau')] \stackrel{\text{def}}{=} \int_{\mathcal{D}_\xi(\tau')} \rho(\xi^1, \dots, \xi^{N_c}) d^N \xi, \quad (20)$$

with $\rho(\xi^1, \dots, \xi^{N_c})$ being the so-called Fisher density. It is equal to the square root of the determinant of the Fisher-Rao information metric tensor $g_{\mu\nu}^{\text{FR}}(\xi)$, that is, $\rho(\xi) \stackrel{\text{def}}{=}} \sqrt{g^{\text{FR}}(\xi)}$ with $g^{\text{FR}}(\xi) \stackrel{\text{def}}{=} \det[g_{\mu\nu}^{\text{FR}}(\xi)]$. Within the continuous microspace setting, recollect that $g_{\mu\nu}^{\text{FR}}(\xi)$ is given by

$$g_{\mu\nu}^{\text{FR}}(\xi) \stackrel{\text{def}}{=} \int p(x|\xi) \partial_\mu \log p(x|\xi) \partial_\nu \log p(x|\xi) dx, \quad (21)$$

where $\partial_\mu \stackrel{\text{def}}{=} \partial/\partial \xi^\mu$ and $1 \leq \mu, \nu \leq N_c$. Interestingly, observe that $\text{vol}[\mathcal{D}_\xi(\tau')]$ in Eq. (20) acquires a simpler form when manifolds are provided with metric tensors characterized by factorizable determinants such as,

$$g(\xi) = g(\xi^1, \dots, \xi^{N_c}) \stackrel{\text{def}}{=} \prod_{k=1}^{N_c} g_k(\xi^k). \quad (22)$$

In such a simplified (i.e., factorizable) scenario, the IGE in Eq. (18) can be recast as

$$\mathcal{S}_{\mathcal{M}_s}(\tau) = \log \left\{ \frac{1}{\tau} \int_0^\tau \left[\prod_{k=1}^{N_c} \left(\int_{\tau_0}^{\tau_0 + \tau'} \sqrt{g_k[\xi^k(\chi)]} \frac{d\xi^k}{d\chi} d\chi \right) \right] d\tau' \right\}. \quad (23)$$

We stress that, when the microvariables $\{x\}$ are correlated, $g(\xi)$ is not factorizable. In this more complicated (i.e., non-factorizable) scenario [56], one needs to employ the general definition of the IGE. In the IGAC framework, the complexity of the statistical models being studied can be specified by the leading asymptotic behavior of $\mathcal{S}_{\mathcal{M}_s}(\tau)$ in Eq. (23). For this reason, we take into consideration the leading asymptotic term in Eq. (18) for the IGE,

$$\mathcal{S}_{\mathcal{M}_s}^{\text{asymptotic}}(\tau) \sim \lim_{\tau \rightarrow \infty} [\mathcal{S}_{\mathcal{M}_s}(\tau)]. \quad (24)$$

The quantity $\mathcal{D}_\xi(\tau')$ defines the domain of integration in the expression of $\text{vol}[\mathcal{D}_\xi(\tau')]$ in Eq. (20). It is given by

$$\mathcal{D}_\xi(\tau') \stackrel{\text{def}}{=} \{\xi : \xi^k(\tau_0) \leq \xi^k \leq \xi^k(\tau_0 + \tau')\}, \quad (25)$$

with $\tau_0 \leq \chi \leq \tau_0 + \tau'$ and τ_0 being the initial value of the affine parameter χ . In Eq. (25), $\xi^k = \xi^k(\chi)$ fulfills the geodesic equation

$$\frac{d^2 \xi^k}{d\chi^2} + \Gamma_{ij}^k \frac{d\xi^i}{d\chi} \frac{d\xi^j}{d\chi} = 0, \quad (26)$$

where Γ_{ij}^k in Eq. (26) are the Christoffel connection coefficients,

$$\Gamma_{ij}^k \stackrel{\text{def}}{=} \frac{1}{2} g^{kl} (\partial_i g_{lj} + \partial_j g_{il} - \partial_l g_{ij}). \quad (27)$$

Observe that $\mathcal{D}_\xi(\tau')$ in Eq. (25) is an N_c -dimensional subspace of $\mathcal{D}_\xi^{\text{tot}}$, with elements being N_c -dimensional macrovariables $\{\xi\}$ whose components ξ^j are bounded by fixed integration limits given by $\xi^j(\tau_0)$ and $\xi^j(\tau_0 + \tau')$. These limits can be found via the integration of the N_c -coupled nonlinear second order ODEs in Eq. (26). Given the IGE, the so-called information geometric complexity (IGC) $\mathcal{C}_{\mathcal{M}_s}(\tau)$ is defined as

$$\mathcal{C}_{\mathcal{M}_s}(\tau) \stackrel{\text{def}}{=} \widetilde{\text{vol}}[\mathcal{D}_\xi(\tau)] = e^{\mathcal{S}_{\mathcal{M}_s}(\tau)}. \quad (28)$$

As previously stated, we shall set our attention on the asymptotic temporal behavior of the IGC as given by $\mathcal{C}_{\mathcal{M}_s}^{\text{asymptotic}}(\tau) \stackrel{\tau \rightarrow \infty}{\sim} e^{\mathcal{S}_{\mathcal{M}_s}(\tau)}$. The interpretation of the IGE $\mathcal{S}_{\mathcal{M}_s}(\tau)$ in Eq. (18) can be used to explain the significance of the IGC $\mathcal{C}_{\mathcal{M}_s}(\tau)$. The IGE is a measure of the number of the accessed macrostates in \mathcal{M}_s defined in terms of the temporal average of the N_c -fold integral of the Fisher density evaluated over geodesics viewed as maximum probability trajectories. Specifically, the instantaneous IGE represents the logarithm of the volume of the parameter space accessed by the system at that particular instant in time. The temporal averaging technique in Eq. (19) is proposed to average out the possibly very intricate fine details of the probabilistic dynamical description of the system on the manifold \mathcal{M}_s . Moreover, the long-time limit in Eq. (24) is employed to conveniently describe the identified dynamical indicators of complexity by disregarding the transient effects which characterize the calculation of the expected value of the volume of the accessed parameter space.

Summing up, the IGE offers an asymptotic coarse-grained inferential description of the complex dynamics of a system in the presence of limited available relevant information. For more in-depth information on the IGC and the IGE, we suggest Refs. [43–46]. Although we limited our discussion to a classical probabilistic continuous setting, our approach can be easily extended to a classical probabilistic discrete setting specified by probability mass functions. Additionally, with some care, it can be extended to quantum probabilistic settings defined by manifolds of parametrized density operators equipped with suitable metrics.

We are now ready to introduce our notions of *complexity* and *complexity length scale* of a quantum evolution for a qubit state.

B. Deterministic quantum setting

In transitioning from the probabilistic classical setting to the deterministic quantum setting for two-levels quantum systems, several differences occur. First, we transition from an (entropic) geodesic motion on an arbitrary N_c -dimensional curved statistical manifold of probability distributions to a (deterministic) quantum temporal evolution (either geodesic or nongeodesic) on a two-dimensional Bloch sphere. Any dynamically evolving unit pure quantum state on this sphere can be parametrized by means of two real parameters, for instance the polar and the azimuthal angles. Second, while the Fisher-Rao information metric is the natural metric on classical statistical manifolds, the Fubini-Study metric is the natural metric on the Bloch sphere. Third, the globally accessible parameter space in

the quantum domain is finite, unlike what generally happens in the classical probabilistic domain. For instance, for a statistical manifold of Gaussian probability distributions, the globally accessible parameter space is not finite. Fourth, we expect fine details to be significantly less intricate than the ones that occur in a classical probabilistic evolution. Nevertheless, the temporal averaging technique can be equally important in the deterministic quantum setting considered here in order to average out possible finer details and keep track of a more relevant overall global behavior of the quantum evolution. Fifth, the entropic nature of the evolution requires the study of the asymptotic temporal behavior of statistical volumes to disregard temporary transient effects and consider only long-lasting effects of the classical probabilistic evolution. Due to the deterministic nature of the quantum evolution that we take into consideration here, this long-time limit is no longer required since there is no necessity to differentiate between (nonpermanent) short-term and (permanent) long-term behaviors. Moreover, we are considering here finite-time quantum processes for which the concept of asymptotic temporal behavior is simply ill-defined.

1. Complexity

Given these preliminary remarks, to quantify the complex behavior of quantum evolutions during a finite time-interval $[t_A, t_B]$, we propose the quantity $C(t_A, t_B)$ defined as

$$C(t_A, t_B) \stackrel{\text{def}}{=} \frac{V_{\max}(t_A, t_B) - \bar{V}(t_A, t_B)}{V_{\max}(t_A, t_B)}. \quad (29)$$

In what follows, we specify the definitions of $\bar{V}(t_A, t_B)$ and $V_{\max}(t_A, t_B)$ in Eq. (29). Furthermore, we justify the reason why we propose $C(t_A, t_B)$ in Eq. (29) as a suitable measure of complexity.

To define the so-called *accessed volume* $\bar{V}(t_A, t_B)$, we schematically proceed as follows. Ideally, integrate the time-dependent Schrödinger evolution equation $i\hbar\partial_t|\psi(t)\rangle = H(t)|\psi(t)\rangle$ and express the (normalized) single-qubit state vector $|\psi(t)\rangle$ at an arbitrary time t in terms of the computational basis state vectors $\{|0\rangle, |1\rangle\}$. We have $|\psi(t)\rangle = c_0(t)|0\rangle + c_1(t)|1\rangle$ with $c_0(t)$ and $c_1(t)$ given by

$$c_0(t) \stackrel{\text{def}}{=} \langle 0|\psi(t)\rangle = |c_0(t)|e^{i\phi_0(t)}, \text{ and } c_1(t) \stackrel{\text{def}}{=} \langle 1|\psi(t)\rangle = |c_1(t)|e^{i\phi_1(t)}, \quad (30)$$

respectively. Furthermore, note that $\phi_0(t)$ and $\phi_1(t)$ are the (real) phases of $c_0(t)$ and $c_1(t)$, respectively. Then, using the complex quantum amplitudes $c_0(t)$ and $c_1(t)$ in Eq. (30), recast the state $|\psi(t)\rangle$ in terms of a physically equivalent state expressed in its canonical Bloch sphere representation specified by the polar angle $\theta(t) \in [0, \pi]$ and the azimuthal angle $\varphi(t) \in [0, 2\pi)$. From the temporal behavior of the two spherical angles, construct the volume of the parametric region accessed by the quantum system during its transition from $|\psi(t_A)\rangle = |A\rangle$ to $|\psi(t)\rangle$. Finally, find the time-average volume of the parametric region accessed by the quantum system during its transition from $|\psi(t_A)\rangle = |A\rangle$ to $|\psi(t_B)\rangle = |B\rangle$ with $t_A \leq t \leq t_B$.

After this preliminary outline, we go in some details here on how to calculate $\bar{V}(t_A, t_B)$. Using Eq. (30), we observe that $|\psi(t)\rangle = c_0(t)|0\rangle + c_1(t)|1\rangle$ is physically equivalent to the state $|c_0(t)||0\rangle + |c_1(t)|e^{i[\phi_1(t) - \phi_0(t)]}|1\rangle$. Thus, $|\psi(t)\rangle$ can be recast as

$$|\psi(t)\rangle = \cos\left(\frac{\theta(t)}{2}\right)|0\rangle + e^{i\varphi(t)}\sin\left(\frac{\theta(t)}{2}\right)|1\rangle. \quad (31)$$

Formally, the polar angle $\theta(t)$ and the azimuthal angle $\varphi(t) \stackrel{\text{def}}{=} \phi_1(t) - \phi_0(t) = \arg[c_1(t)] - \arg[c_0(t)]$ in Eq. (31) are given by,

$$\theta(t) \stackrel{\text{def}}{=} 2 \arctan\left(\frac{|c_1(t)|}{|c_0(t)|}\right), \quad (32)$$

and, assuming $\text{Re}[c_1(t)] > 0$ and $\text{Re}[c_0(t)] > 0$,

$$\varphi(t) \stackrel{\text{def}}{=} \arctan\left\{\frac{\text{Im}[c_1(t)]}{\text{Re}[c_1(t)]}\right\} - \arctan\left\{\frac{\text{Im}[c_0(t)]}{\text{Re}[c_0(t)]}\right\}, \quad (33)$$

respectively. More generally, the expression for $\varphi(t)$ in Eq. (33) can become more complicated. This is due to the fact that, in general, the phase $\arg(z)$ of a complex number $\mathbb{C} \ni z \stackrel{\text{def}}{=} x + iy = |z|e^{i\arg(z)}$ must be expressed by means of the 2-argument arctangent function atan2 as $\arg(z) = \text{atan2}(y, x)$. When $x > 0$, $\text{atan2}(y, x)$ reduces to $\arctan(y/x)$. For more details, we refer to Ref. [57]. Then, the unit Bloch vector $\hat{r}(t)$ that corresponds to the state

vector $|\psi(t)\rangle$ in Eq. (31) equals $\hat{r}(t) = (\sin[\theta(t)] \cos[\varphi(t)], \sin[\theta(t)] \sin[\varphi(t)], \cos[\theta(t)])$. We are now in a position where we can define $\bar{V}(t_A, t_B)$. Namely, the accessed volume $\bar{V}(t_A, t_B)$ that corresponds to the quantum evolution from $|\psi(t_A)\rangle = |A\rangle$ to $|\psi(t_B)\rangle = |B\rangle$, with $t_A \leq t \leq t_B$, under the Hamiltonian $H(t)$, is defined as

$$\bar{V}(t_A, t_B) \stackrel{\text{def}}{=} \frac{1}{t_B - t_A} \int_{t_A}^{t_B} V(t) dt. \quad (34)$$

The quantity $V(t)$ in Eq. (34) is the instantaneous volume given by,

$$V(t) = V(\theta(t), \varphi(t)) \stackrel{\text{def}}{=} \text{vol}[\mathcal{D}_{\text{accessed}}[\theta(t), \varphi(t)]], \quad (35)$$

with $\text{vol}[\mathcal{D}_{\text{accessed}}[\theta(t), \varphi(t)]]$ being defined as,

$$\text{vol}[\mathcal{D}_{\text{accessed}}[\theta(t), \varphi(t)]] \stackrel{\text{def}}{=} \int \int_{\mathcal{D}_{\text{accessed}}[\theta(t), \varphi(t)]} \sqrt{g_{\text{FS}}(\theta, \varphi)} d\theta d\varphi. \quad (36)$$

We reiterate that we take these volumes to be positive quantities. Therefore, whenever we write $\text{vol}[\cdot]$, we really mean $|\text{vol}[\cdot]| \geq 0$. In Eq. (36), $g_{\text{FS}}(\theta, \varphi) \stackrel{\text{def}}{=} \sqrt{\sin^2(\theta)/16}$ is the determinant of the matrix that corresponds to the Fubini-Study infinitesimal line element $ds_{\text{FS}}^2 \stackrel{\text{def}}{=} (1/4) [d\theta^2 + \sin^2(\theta) d\varphi^2]$. Finally, $\mathcal{D}_{\text{accessed}}[\theta(t), \varphi(t)]$ in Eq. (36) specifies the parametric region accessed by the quantum system during its transition from the initial state $|\psi(t_A)\rangle = |A\rangle$ to an intermediate state $|\psi(t)\rangle$, with $t_A \leq t \leq t_B$. It is defined as

$$\mathcal{D}_{\text{accessed}}[\theta(t), \varphi(t)] \stackrel{\text{def}}{=} [\theta(t_A), \theta(t)] \times [\varphi(t_A), \varphi(t)] \subset [0, \pi]_{\theta} \times [0, 2\pi]_{\varphi}. \quad (37)$$

For computational convenience, we remark that the instantaneous volume $V(t)$ in Eq. (35) can be simply expressed as $V(t) = |(\cos[\theta(t_A)] - \cos[\theta(t)])(\varphi(t) - \varphi(t_A))|/4$ with $\theta(t)$ and $\varphi(t)$ in Eqs. (32) and (33), respectively. In conclusion, inspired by our classical probabilistic setting (where the tilde symbol is used to denote the time-average procedure), the accessed volume $\bar{V}(t_A, t_B)$ in Eq. (34) can be recast as

$$\bar{V}(t_A, t_B) \stackrel{\text{def}}{=} \widetilde{\text{vol}}[\mathcal{D}_{\text{accessed}}[\theta(t), \varphi(t)]], \quad (38)$$

with $t_A \leq t \leq t_B$ in Eq. (38).

To introduce the so-called *accessible volume* $V_{\text{max}}(t_A, t_B)$, we need to present some preliminary remarks. The departure, with respect to the classical probabilistic setting, from the focus on the asymptotic temporal behavior of the complexity measure together with the boundedness of the globally accessible parametric regions demand some care. Indeed, these two aspects, along with the fact that we are now interested in comparing the complexity of distinct quantum evolutions connecting the same pair of initial and final states, lead us to consider a notion of quantum complexity length scale.

We recall that the idea that complexity is more than length appears in different fields of science, including computer science [58–60] and evolutionary biology [61]. For instance, when defining the concept of software complexity in computer science, one can argue that the complexity should be an attribute that measures something independent of the length of a software program [60]. For example, complexity might increase with the size of the task, but this increase should usually be less than the increase in size. Furthermore, when defining the notion of evolutionary complexity in biology, one observes that there can be large variations in the so-called size-complexity rule [61]. Indeed, the relationship between size (or, alternatively, length) and complexity can be quite complicated when investigating the evolution of biological systems such as small multicellular organisms. For such systems, for example, an increase or decrease in complexity does not necessarily require changes in size. Finally, for an interesting discussion on how complexity should scale with size in an information theory characterization of physical systems, we suggest Ref. [20]. Then, keeping in mind that complexity is more than length, we propose to construct a quantum complexity length scale as a product of two main factors. The first factor is the actual length of the path on the Bloch sphere that connects the given initial and final states. Clearly, different Hamiltonians yield different paths with different lengths during the evolution in a finite time interval $t_B - t_A$. The second factor, instead, takes into account the fact that different Hamiltonians give rise to different bounded accessed volumes of parametric regions where each one can be “boxed” with a corresponding greater (yet bounded) local accessible volume. The ratio between these two volumes, in turn, can be regarded as a sort of normalized (local) volume ratio that will specify the second factor in our proposed quantum complexity length scale discussed in the next subsection. Given this set of remarks, we define the accessible volume $V_{\text{max}}(t_A, t_B)$ as

$$V_{\text{max}}(t_A, t_B) \stackrel{\text{def}}{=} \text{vol}[\mathcal{D}_{\text{accessible}}(\theta, \varphi)] = \int \int_{\mathcal{D}_{\text{accessible}}(\theta, \varphi)} \sqrt{g_{\text{FS}}(\theta, \varphi)} d\theta d\varphi. \quad (39)$$

The quantity $\mathcal{D}_{\text{accessible}}(\theta, \varphi)$ in Eq. (39) is the (local) maximally accessible two-dimensional parametric region during the quantum evolution from $|\psi_A(\theta_A, \varphi_A)\rangle$ to $|\psi(\theta_B, \varphi_B)\rangle$ and is defined as

$$\mathcal{D}_{\text{accessible}}(\theta, \varphi) \stackrel{\text{def}}{=} \{(\theta, \varphi) : \theta_{\min} \leq \theta \leq \theta_{\max}, \text{ and } \varphi_{\min} \leq \varphi \leq \varphi_{\max}\}. \quad (40)$$

Note that θ_{\min} , θ_{\max} , φ_{\min} , and φ_{\max} in Eq. (40) are given by

$$\theta_{\min} \stackrel{\text{def}}{=} \min_{t_A \leq t \leq t_B} \theta(t), \theta_{\max} \stackrel{\text{def}}{=} \max_{t_A \leq t \leq t_B} \theta(t), \varphi_{\min} \stackrel{\text{def}}{=} \min_{t_A \leq t \leq t_B} \varphi(t), \text{ and } \varphi_{\max} \stackrel{\text{def}}{=} \max_{t_A \leq t \leq t_B} \varphi(t), \quad (41)$$

respectively. Furthermore, observe that we have $\mathcal{D}_{\text{accessed}}(\theta, \varphi) \subset \mathcal{D}_{\text{accessible}}(\theta, \varphi) \subset [0, \pi]_{\theta} \times [0, 2\pi]_{\varphi}$. Finally, given $\bar{V}(t_A, t_B)$ and $V_{\max}(t_A, t_B)$ in Eqs. (34) and (39), respectively, our proposed concept of complexity $C(t_A, t_B)$ in Eq. (29) is formally defined. It is worthwhile pointing out here that in the context of Bayesian model selection, the so-called Bayesian complexity is formally defined as the natural logarithm of the ratio between two volumes, $C_{\text{Bayesian}} \stackrel{\text{def}}{=} \ln[V(f)/V_c(f)]$ [62]. The quantities $V_c(f)$ and $V(f)$ denote the volume of the distinguishable distributions in f that come close to the truth and the total volume of the model family f , respectively. In particular, a small ratio $V_c(f)/V(f)$ specifies (complex) models that occupy a small volume close to the truth relative to the total volume of the model. For this reason, a complex model (in a Bayesian sense) is one with a small fraction of its distinguishable probability distributions lying near the truth [62]. Similarly, identifying $V_c \leftrightarrow \bar{V}$ and $V \leftrightarrow V_{\max}$, the ratio \bar{V}/V_{\max} is introduced to compare in a meaningful way different Hamiltonian evolutions. These, in turn, can be possibly specified by parametric regions of different dimension. Furthermore, the ratio \bar{V}/V_{\max} penalizes Hamiltonian evolutions with a corresponding accessed (i.e., occupied) parametric region of volume equal to only a small fraction of the accessible volume. Lastly, a complex quantum Hamiltonian evolution is one with a small fraction \bar{V}/V_{\max} , i.e. with a large fraction $(V_{\max} - \bar{V})/V_{\max}$.

For clarity, it is worthwhile pointing out that the $C(t_A, t_B)$ in Eq. (29) is well-defined for a quantum evolution that occurs along a meridian (specified by a constant φ) or a parallel (characterized by a constant θ). For clarity of exposition, consider the evolution from an initial state $|A\rangle \stackrel{\text{def}}{=} [|0\rangle + |1\rangle]/\sqrt{2}$ to a final state $|B\rangle \stackrel{\text{def}}{=} |A\rangle = [|0\rangle + i|1\rangle]/\sqrt{2}$ under an Hamiltonian of the form $H \stackrel{\text{def}}{=} E\sigma_z$ with $E \stackrel{\text{def}}{=} \hbar\omega$. During this evolution from $t_A = 0$ to $t_B = \pi/(4\omega)$, $\theta(t) = \pi/2$ (i.e., a parallel on the Bloch sphere) and $\varphi(t) = 2\omega t$ for any $t_A \leq t \leq t_B$. Furthermore, a simple calculation yields $\bar{V}(t_A, t_B) = \pi/8$ and $V_{\max}(t_A, t_B) = \pi/4$. Thus, $C(t_A, t_B) = 1/2$. A consistency check, we emphasize that we expect to obtain the same complexity for a quantum evolution from an initial state $|A\rangle \stackrel{\text{def}}{=} [|0\rangle + i|1\rangle]/\sqrt{2}$ to a final state $|B\rangle \stackrel{\text{def}}{=} |0\rangle$ under an Hamiltonian of the form $H \stackrel{\text{def}}{=} E\sigma_x$ with $E \stackrel{\text{def}}{=} \hbar\omega$. During this evolution from $t_A = 0$ to $t_B = \pi/(4\omega)$, $\theta(t) = 2 \arctan \left[\sqrt{\left(\frac{\cos(\omega t) - \sin(\omega t)}{\cos(\omega t) + \sin(\omega t)} \right)^2} \right]$ and $\varphi(t) = \pi/2$ (i.e., a meridian on the Bloch sphere) for any $t_A \leq t \leq t_B$. Again, a simple calculation leads to $\bar{V}(t_A, t_B) = \pi/8$ and $V_{\max}(t_A, t_B) = \pi/4$. Thus, as expected on physical grounds, $C(t_A, t_B) = 1/2$ as in the previous illustrative example.

In Fig. 3, we provide an intuitive picture to help grasping the meaning of the concept of complexity proposed in Eq. (29).

Having proposed a notion of complexity for a quantum evolution, we can introduce now the concept of complexity length scale.

2. Complexity length scale

We begin by recalling the concept of length of a path on the Bloch sphere. To describe the physical significance of the Riemannian distance between two arbitrarily selected pure quantum states, we suggest the work by Wootters in Ref. [35]. For mixed states, instead, we suggest the analysis carried out by Braunstein and Caves in Ref. [32]. Given two infinitesimally close points ξ and $\xi + d\xi$ along a path $\xi(\chi)$ with $\chi_1 \leq \chi \leq \chi_2$, they can be considered statistically distinguishable if $d\xi$ is greater than (or equal to) the standard fluctuation of ξ [63]. In general, the infinitesimal line element along the path equals ds_{FS} with $ds_{\text{FS}}^2 = g_{\mu\nu}^{\text{FS}}(\xi) d\xi^\mu d\xi^\nu$ with $1 \leq \mu, \nu \leq m$, where m represents the number of real parameters used to parametrize the quantum state. The length \mathcal{L} of the path $\xi(\chi)$ with $\chi_1 \leq \chi \leq \chi_2$ between $\xi_1 \stackrel{\text{def}}{=} \xi(\chi_1)$ and $\xi_2 \stackrel{\text{def}}{=} \xi(\chi_2)$ is given by

$$\mathcal{L} \stackrel{\text{def}}{=} \int_{\xi_1}^{\xi_2} \sqrt{ds_{\text{FS}}^2} = \int_{\chi_1}^{\chi_2} \sqrt{\frac{ds_{\text{FS}}^2}{d\chi^2}} d\chi, \quad (42)$$

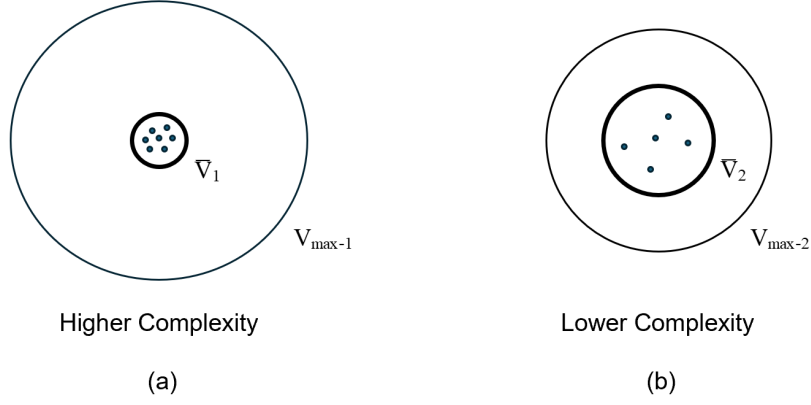


FIG. 3: Schematic depiction that helps grasping the concept of complexity C in Eq. (29). In (a), we sketch a complex scenario where the accessed volume \bar{V}_1 (region enclosed by the thick circular line) is a small fraction of the accessible volume $V_{\max-1}$ (region enclosed by the thin circular line). In (b), instead, we describe a scenario with a smaller degree of complexity since \bar{V}_2 (region enclosed by the thick circular line) is a larger fraction of $V_{\max-2}$ (region enclosed by the thin circular line). In general, to a higher complexity scenario there corresponds a long quantum path of length s_1 specified by a small fraction ($\bar{V}_1/V_{\max-1}$) of the accessible volume $V_{\max-1}$. To a lower complexity scenario, instead, there corresponds a short quantum path of length $s_2 < s_1$ described by a large fraction ($\bar{V}_2/V_{\max-2}$, with $\bar{V}_2/V_{\max-2} > \bar{V}_1/V_{\max-1}$) of the accessible volume $V_{\max-2}$. The number of points depicted in an accessed volume \bar{V} is taken here to be proportional to the squared length of the path s^2 amplified by a (greater than one) factor which is the reciprocal of \bar{V}/V_{\max} with $0 \leq \bar{V}/V_{\max} \leq 1$. These two scenarios are well-described by the notion of complexity length scale L_C in Eq. (44), with $L_C^2 = s^2 \cdot (\bar{V}/V_{\max})^{-1}$.

and denotes the maximal number \tilde{N} of statistically distinguishable quantum states along the path $\xi(\chi)$. For two-level quantum systems, $ds_{\text{FS}}^2 \stackrel{\text{def}}{=} (1/4) [d\theta^2 + \sin^2(\theta)d\varphi^2]$. Interestingly, the geodesic distance between ξ_1 and ξ_2 represents the path of shortest distance between ξ_1 and ξ_2 and is given by the minimum of \tilde{N} . This link between path length and number of statistically distinguishable states along the path is a significant physical consideration to keep in mind throughout our analysis. Besides, this perspective can be generalized in a natural fashion to the geometric characterization of quantum mixed states [32]. More explicitly, from a geodesic efficiency standpoint, we know that an efficient quantum evolution is the one with a length of the path s given by [38],

$$s \stackrel{\text{def}}{=} \int_{t_A}^{t_B} 2 \frac{\Delta E(t)}{\hbar} dt, \quad (43)$$

connecting an initial (i.e., $|\psi_A(\theta_A, \varphi_A)\rangle$) and a final (i.e., $|\psi_B(\theta_B, \varphi_B)\rangle$) quantum state as small as possible (that is, with the length as close as possible to the shortest geodesic path length $s_0 \stackrel{\text{def}}{=} 2 \arccos [|\langle \psi_A(\theta_A, \varphi_A) | \psi_B(\theta_B, \varphi_B) \rangle|]$ connecting the two states). The quantity $\Delta E(t)$ in Eq. (43) is the energy uncertainty (i.e., the square-root of the variance of the Hamiltonian operator with respect to the state $|\psi(t)\rangle$). Therefore, ranking quantum evolutions in terms of the geodesic efficiency $\eta_{\text{GE}} \stackrel{\text{def}}{=} s_0/s$ [38, 39]) is straightforward. At the same time, one might ask if it is reasonable to expect that the most efficient quantum evolution occurs by exploring the (smallest) average volume of the accessed parametric region in the shortest possible time. Unlike what one might be tempted to think from the classical probabilistic approach, it turns out that ranking the performance of quantum evolutions is more subtle than expected when one takes into account the average volume of the accessed parametric region (i.e., the accessed volume $\bar{V}(t_A, t_B)$ in Eq. (34)) together with the maximum volume of the accessible parametric region specified by the accessible volume $V_{\max}(t_A, t_B)$ in Eq. (39).

In the spirit that complexity is more than length, we express in a quantitative manner this subtlety by introducing a so-called *complexity length scale* $L_C(t_A, t_B) \geq s(t_A, t_B)$ for any quantum evolution specified by a length s of the path connecting an initial and a final quantum state $|\psi_A(\theta_A, \varphi_A)\rangle$ and $|\psi_B(\theta_B, \varphi_B)\rangle$, respectively. Finally, we define L_C as

$$L_C(t_A, t_B) \stackrel{\text{def}}{=} \frac{s(t_A, t_B)}{\sqrt{\frac{\bar{V}(t_A, t_B)}{V_{\max}(t_A, t_B)}}}, \quad (44)$$

α	$\bar{V}(\alpha)$	$V_{\max}(\alpha)$	$C(\alpha)$	$L_C(\alpha)$	$\pi - \alpha$
0	0.1917	0.2777	0.3096	2.6735	π
$\frac{1}{16}\pi$	0.1536	0.2243	0.3152	2.3996	$\frac{15}{16}\pi$
$\frac{1}{8}\pi$	0.1064	0.1765	0.3973	2.3509	$\frac{7}{8}\pi$
$\frac{3}{16}\pi$	0.0508	0.1358	0.6259	2.8135	$\frac{13}{16}\pi$
$\frac{1}{4}\pi$	0.0333	0.1016	0.6719	2.8888	$\frac{3}{4}\pi$
$\frac{5}{16}\pi$	0.0238	0.0723	0.6710	2.8128	$\frac{11}{16}\pi$
$\frac{3}{8}\pi$	0.0153	0.0465	0.6706	2.7674	$\frac{5}{8}\pi$
$\frac{7}{16}\pi$	0.0075	0.0228	0.6705	2.7439	$\frac{9}{16}\pi$
$\frac{1}{2}\pi$	0.3927	0.7854	0.5	2.2214	$\frac{1}{2}\pi$

TABLE I: Numerical estimates of the accessed volume $\bar{V}(\alpha)$, the accessible volume $V_{\max}(\alpha)$, the complexity $C(\alpha)$, and the complexity length scale $L_C(\alpha)$ for $\alpha \in [0, \pi]$. The interval $[0, \pi]$ was partitioned into sixteen sub-intervals of equal size $\pi/16$. Note that $\bar{V}(\alpha)$ and $V_{\max}(\alpha)$ assume the same numerical values for the angles α and the corresponding supplementary angles $\pi - \alpha$. This symmetry is expected on physical grounds.

that is, using Eqs. (34), (43), and (39),

$$L_C(t_A, t_B) \stackrel{\text{def}}{=} \left(\int_{t_A}^{t_B} 2 \frac{\Delta E(t)}{\hbar} dt \right) \left(\frac{\frac{1}{t_B - t_A} \int_{t_A}^{t_B} \left| \int_{\mathcal{D}_{\text{accessed}}(\theta, \varphi)} \sqrt{g_{\text{FS}}(\theta, \varphi)} d\theta d\varphi \right| dt}{\left| \int_{\mathcal{D}_{\text{accessible}}(\theta, \varphi)} \sqrt{g_{\text{FS}}(\theta, \varphi)} d\theta d\varphi \right|} \right)^{-1/2}. \quad (45)$$

The quantity $L_C(t_A, t_B)$ in Eq. (45) is the proposed quantum complexity length scale for a quantum evolution that happens in a finite time interval $t_B - t_A$. From a dimensional analysis standpoint, Eq. (44) can be seen as emerging from the educated guess, $s^2 : \bar{V} = L_C^2 : V_{\max}$. Although we have been using the word ‘‘volume’’ in this paper, these parametric regions in Eqs. (37) and (40) are actually two-dimensional. Loosely speaking, our intuitive perspective behind our proposed complexity quantum length scale definition in Eq. (44) can be summarized as follows. For a given pair of initial and final quantum states on the Bloch sphere, describing a shorter path that connects these two states with an accessed parameter space that is a big fraction of the locally accessible parameter space is less complex than describing a longer path with an accessed parameter space that is only a small fraction of the locally accessible parameter space. This length scale L_C is meant to capture the following intuitive point: A longer path that occupies a smaller fraction of the maximum volume of the accessible parametric region is more complex than a shorter path that occupies a larger fraction of the available parametric region. In principle, a more efficient quantum evolution need not to be necessarily a less complex quantum evolution (i.e., $s_1 \leq s_2$ does not necessarily imply $L_{C_1} \leq L_{C_2}$). Indeed, a less complex quantum evolution is not necessarily the one that goes through a smaller average accessed volume in a shorter time. Rather, it is the one for which the average accessed volume is as close as possible to the maximum accessible volume. Our proposed complexity length scale takes into account both effects, i.e. the length of the path and the ratio between accessed and accessible volumes (or, in other words, the complexity of the evolution). Indeed, using Eqs. (29) and (44), an alternative representation of L_C is

$$L_C(t_A, t_B) = \frac{s(t_A, t_B)}{\sqrt{1 - C(t_A, t_B)}}. \quad (46)$$

From Eq. (46), we see that $L_C(t_A, t_B) \geq s(t_A, t_B)$ since $0 \leq C(t_A, t_B) \leq 1$ by construction. Furthermore, it is interesting to note that $s_2(t_A, t_B) \geq s_1(t_A, t_B)$ does not imply necessarily that $L_{C_2}(t_A, t_B) \geq L_{C_1}(t_A, t_B)$. Indeed, if $C_2(t_A, t_B)$ is sufficiently smaller than $C_1(t_A, t_B)$ and, in addition, $s_2(t_A, t_B)$ is not too much greater than $s_1(t_A, t_B)$, we can still have $L_{C_2}(t_A, t_B) \leq L_{C_1}(t_A, t_B)$. Thus, the complexity length scale of quantum evolutions yielding longer paths can be smaller than the complexity length scale of evolutions leading to shorter paths, provided that their corresponding accessed volumes are as close as possible to their accessible volumes. (i.e., $C(t_A, t_B)$ as small as possible).

We are now ready to apply our proposed measure of complexity $C(t_A, t_B)$ in Eq. (29) and quantum complexity length scale $L_C(t_A, t_B)$ in Eq. (44) to actual physical evolutions for a two-level quantum system.

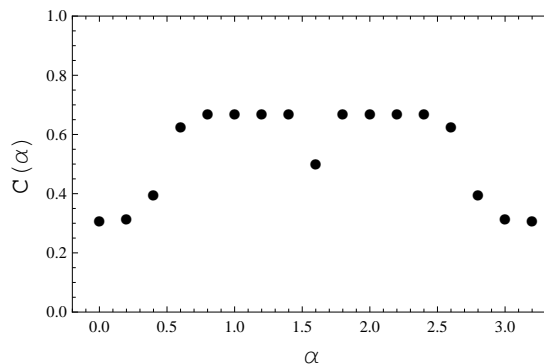


FIG. 4: Scatter plot of the complexity $C(\alpha)$ versus α , with $\alpha \in [0, \pi]$. The numerical estimates for $C(\alpha)$ appear in Table I. For values of α in the interval centered at $\pi/2$ and radius $\pi/4$, i.e. in $[\pi/4, (3/4)\pi]$, the complexity $C(\alpha)$ assumes its local minimum value of 0.5 at $\alpha = \pi/2$. However, the complexity of Hamiltonian evolutions with α sufficiently far from $\pi/2$ can assume values smaller than 0.5. Recalling that a complex Hamiltonian model is one with a small fraction $\bar{V}(\alpha)/V_{\max}(\alpha)$, this behavior can be ascribed to the fact that these Hamiltonians $H_{\text{sub-opt}}(\alpha)$ yield longer paths connecting initial and final states and tend to occupy a large fraction of the accessible volume.

IV. COMPLEXITY OF HAMILTONIAN EVOLUTIONS

In this section, we numerically estimate the complexity measure $C(t_A, t_B)$ in Eq. (29) and the complexity length scale $L_C(t_A, t_B)$ in Eq. (44) for H_{opt} in Eq. (1) and several members of the family of Hamiltonians $H_{\text{sub-opt}}(\alpha)$ in Eq. (8) with $0 \leq \alpha \leq \pi$.

In what follows, we assume for illustrative purposes to consider quantum evolutions from the initial state $|A\rangle \stackrel{\text{def}}{=} [|0\rangle + |1\rangle]/\sqrt{2}$ with corresponding Bloch vector $\hat{a} \stackrel{\text{def}}{=} (1, 0, 0)$ to the final state $|B\rangle \stackrel{\text{def}}{=} [|0\rangle + i|1\rangle]/\sqrt{2}$ with corresponding Bloch vector $\hat{b} \stackrel{\text{def}}{=} (0, 1, 0)$. Note that $\hat{a} \cdot \hat{b} = \cos(\theta_{AB}) = 0$ since $\theta_{AB} = \pi/2$. Using the optimal Hamiltonian H_{opt} in Eq. (1), it turns out that an intermediate state at time $t \in [t_A, t_B]$ is physically equivalent to the state $|\psi(t)\rangle = (1/\sqrt{2})|0\rangle + (1/\sqrt{2})e^{2i\omega t}|1\rangle$ (with $\omega \stackrel{\text{def}}{=} E/\hbar$). Therefore, the spherical angles become $\theta(t) = \pi/2$ and $\varphi(t) = 2\omega t$. Furthermore, as a consistency check, we point out that $t_{\text{opt}} = [\hbar/(2E)]\theta_{AB} = \pi/(4\omega)$ and $|\psi(t_{\text{opt}})\rangle = [|0\rangle + i|1\rangle]/\sqrt{2} = |B\rangle$. In the sub-optimal scenario, using the sub-optimal Hamiltonian in Eq. (8) and standard quantum-mechanical rules, the unitary evolution operator becomes

$$U_{\text{sub-optimal}}(t) \stackrel{\text{def}}{=} \begin{pmatrix} \cos(\omega t) - i \sin(\alpha) \sin(\omega t) & -\frac{\cos(\alpha)}{\sqrt{2}}(1+i) \sin(\omega t) \\ \frac{\cos(\alpha)}{\sqrt{2}}(1-i) \sin(\omega t) & \cos(\omega t) + i \sin(\alpha) \sin(\omega t) \end{pmatrix}. \quad (47)$$

Applying $U_{\text{sub-optimal}}(t)$ to the initial state $|A\rangle$, the intermediate state $|\psi(t)\rangle = U_{\text{sub-optimal}}(t)|A\rangle$ can be recast as $|\psi(t)\rangle = c_0(t)|0\rangle + c_1(t)|1\rangle$. After some algebra, the complex probability amplitudes $c_0(t) = c_0(t; \alpha, \omega)$ and $c_1(t) = c_1(t; \alpha, \omega)$ can be expressed as

$$c_0(t; \alpha, \omega) \stackrel{\text{def}}{=} \left(\frac{\cos(\omega t)}{\sqrt{2}} - \frac{\cos(\alpha) \sin(\omega t)}{2} \right) + i \left(-\frac{\cos(\alpha) \sin(\omega t)}{2} - \frac{\sin(\alpha) \sin(\omega t)}{\sqrt{2}} \right), \quad (48)$$

and,

$$c_1(t; \alpha, \omega) \stackrel{\text{def}}{=} \left(\frac{\cos(\omega t)}{\sqrt{2}} + \frac{\cos(\alpha) \sin(\omega t)}{2} \right) + i \left(-\frac{\cos(\alpha) \sin(\omega t)}{2} + \frac{\sin(\alpha) \sin(\omega t)}{\sqrt{2}} \right). \quad (49)$$

As a side remark, we note that $|c_0(t)|^2 + |c_1(t)|^2 = 1$. Moreover, $c_0(t) \rightarrow (1/\sqrt{2})e^{-i\omega t}$ and $c_1(t) \rightarrow (1/\sqrt{2})e^{i\omega t}$ as α approaches $\pi/2$, as expected. Using Eqs. (32), (33), (48), and (49), we get

$$\theta(t; \alpha, \omega) \stackrel{\text{def}}{=} 2 \arctan \left\{ \sqrt{\frac{\frac{1}{2} - \frac{\sin(2\alpha)}{2\sqrt{2}} \sin^2(\omega t) + \frac{\cos(\alpha)}{2\sqrt{2}} \sin(2\omega t)}{\frac{1}{2} + \frac{\sin(2\alpha)}{2\sqrt{2}} \sin^2(\omega t) - \frac{\cos(\alpha)}{2\sqrt{2}} \sin(2\omega t)}} \right\}, \quad (50)$$

and,

$$\varphi(t; \alpha, \omega) \stackrel{\text{def}}{=} \arctan \left[\frac{\frac{\sin(\alpha) \sin(\omega t)}{\sqrt{2}} - \frac{\cos(\alpha) \sin(\omega t)}{2}}{\frac{\cos(\alpha) \sin(\omega t)}{2} + \frac{\cos(\omega t)}{\sqrt{2}}} \right] - \arctan \left[\frac{\frac{\cos(\alpha) \sin(\omega t)}{2} + \frac{\sin(\alpha) \sin(\omega t)}{\sqrt{2}}}{\frac{\cos(\alpha) \sin(\omega t)}{2} - \frac{\cos(\omega t)}{\sqrt{2}}} \right]. \quad (51)$$

As a first consistency check, note that we correctly get $\theta(0; \alpha, \omega) = \pi/2$ and $\varphi(0; \alpha, \omega) = 0$. However, we must keep in mind that the expression for $\varphi(t)$ in Eq. (51) can become more complicated. As we previously mentioned, this is caused by the fact that the phase $\arg(z)$ of a complex number $\mathbb{C} \ni z \stackrel{\text{def}}{=} x + iy = |z| e^{i \arg(z)}$ must be generally expressed by means of the 2-argument arctangent function atan2 as $\arg(z) = \text{atan2}(y, x)$. When $x > 0$, $\text{atan2}(y, x)$ reduces to $\arctan(y/x)$. This point is especially important in the numerical estimations of the complexity. For more details, we refer to Appendix A (Complexity Symmetries) and Appendix B (Complexity Calculations). Then, using Eqs. (50), (51), and (35), the time-dependent volume $V(t)$ in Eq. (35) reduces to

$$V(t; \alpha, \omega) = \frac{1}{4} |\varphi(t; \alpha, \omega) \cos[\theta(t; \alpha, \omega)]|, \quad (52)$$

given that $\varphi(0; \alpha, \omega) = 0$ and $\theta(0; \alpha, \omega) = \pi/2$. From Eq. (52), one can calculate the accessed volume $\bar{V}(\alpha, \omega)$ in Eq. (34) and obtain

$$\bar{V}(\alpha, \omega) \stackrel{\text{def}}{=} \frac{1}{t_{\text{sub-opt}}} \int_0^{t_{\text{sub-opt}}} V(t; \alpha, \omega) dt, \quad (53)$$

where $t_{\text{sub-opt}} = t_{\text{sub-opt}}(\alpha, \omega)$ is given in Eq. (11). Using Eqs. (32), (33), and (11), one can also numerically calculate the lower and upper bounds in Eq. (41). Then, one uses these bounds to estimate the accessible volume $V_{\text{max}}(\alpha, \omega)$ in Eq. (39). Finally, having an estimate of $\bar{V}(\alpha, \omega)$, $V_{\text{max}}(\alpha, \omega)$, and $s(\alpha)$ in Eq. (12), one can arrive at the numerical estimates for the complexity $C(\alpha, \omega) \stackrel{\text{def}}{=} [V_{\text{max}}(\alpha, \omega) - \bar{V}(\alpha, \omega)] / V_{\text{max}}(\alpha, \omega)$ in Eq. (29) and the complexity length scale $L_C(\alpha, \omega) \stackrel{\text{def}}{=} s(\alpha) / \sqrt{1 - C(\alpha, \omega)}$ in Eq. (44). In Table I, we set $\omega = 1$ and report the numerical estimates of the accessed volume $\bar{V}(\alpha)$, the accessible volume $V_{\text{max}}(\alpha)$, the complexity $C(\alpha)$, and the complexity length scale $L_C(\alpha)$ for $0 \leq \alpha \leq \pi$. Furthermore, we keep $\omega = 1$ and illustrate in Figs. 4 and 5 the scatter plots of the complexity $C(\alpha)$ and the complexity length scale $L_C(\alpha)$ versus α , respectively. Finally, in Table II, we maintain $\omega = 1$ and display the numerical estimates of the geodesic efficiency $\eta_{\text{GE}}(\alpha)$ in Eq. (13), the speed efficiency $\eta_{\text{SE}}(\alpha)$ in Eq. (14), the curvature coefficient $\kappa_{\text{AC}}^2(\alpha)$ in Eq. (15), the complexity $C(\alpha)$ in Eq. (29), and the complexity length scale $L_C(\alpha)$ in Eq. (44) for $0 \leq \alpha \leq \pi$. Interestingly, we point out that when inspecting the numerical estimates in Table II, one can notice that the curvature coefficient $\kappa_{\text{AC}}^2(\alpha)$ versus the efficiencies $\eta_{\text{GE}}(\alpha)$ or $\eta_{\text{SE}}(\alpha)$ exhibits a monotonically decreasing behavior. Instead, the complexity $C(\alpha)$ and the complexity length scale $L_C(\alpha)$ display a non-monotonic behavior when viewed as functions of $\eta_{\text{GE}}(\alpha)$ or $\eta_{\text{SE}}(\alpha)$. Additional remarks on these intriguing trends appear in the next section. It is also important to point out that for the class of Hamiltonian evolutions analyzed here, the accessed volume $\bar{V}(\alpha, \omega)$ and the accessible volume $V_{\text{max}}(\alpha, \omega)$ do not depend on $\omega \stackrel{\text{def}}{=} E/\hbar$. Furthermore, it happens that $\bar{V}(\alpha) = \bar{V}(\pi - \alpha)$ and $V_{\text{max}}(\alpha) = V_{\text{max}}(\pi - \alpha)$. Thus, the complexity $C(\alpha)$ and the complexity length scale $L_C(\alpha)$ possess identical values for supplementary angles α and $\pi - \alpha$ for any choice of the value for the frequency ω (or, alternatively, for any finite energy value E). These symmetries are discussed in Appendix A. Instead, technical details on the numerical estimates of $C(\alpha)$ can be found in Appendix B.

We are now ready for our summary of results and final remarks.

V. CONCLUDING REMARKS

In this paper, we studied the complexity of both time optimal (Eq. (1)) and time sub-optimal (Eq. (8)) quantum Hamiltonian evolutions connecting arbitrary source and target states on the Bloch sphere equipped with the Fubini-Study metric. This study was conducted in several steps. Initially, we characterized each unitary Schrödinger quantum evolution by quantifying its path length (Eq. (12)), geodesic efficiency (Eq. (13)), speed efficiency (Eq. (14)), and curvature coefficient (Eq. (15)). These quantities were used to describe the dynamical trajectory connecting the source state to the target state (Fig. 2). Next, we went from a classical probabilistic framework, where the complexity of entropic motion on curved statistical manifolds can be described using the information geometric complexity in Eq. (28), to a deterministic quantum setting. In this context, we proposed a definition of quantum evolution complexity (Eq. (29) and Fig. 3) and introduced the concept of a quantum complexity length scale (Eq. (44)). We discussed the physical significance of these quantities in terms of the partial (i.e., accessed volume in Eq. (34)) and total (i.e.,

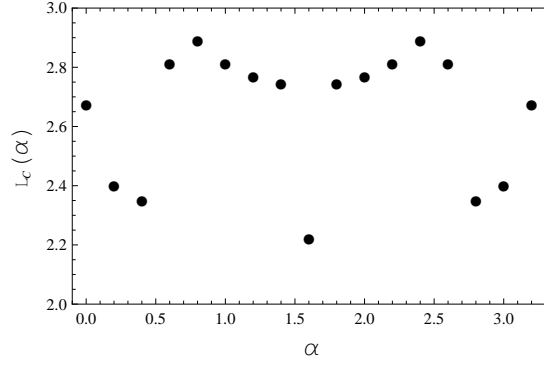


FIG. 5: Scatter plot of the complexity length scale $L_C(\alpha)$ versus α , with $\alpha \in [0, \pi]$. The numerical estimates for $C(\alpha)$ appear in Table I. The minimum value of $L_C(\alpha)$ is obtained at $\alpha = \pi/2 \simeq 1.57$. Focusing on the interval with $\alpha \in [0, \pi/2]$, we note that $L_C(\alpha)$ exhibits a non-monotonic behavior. In particular, the complexity length scale of Hamiltonian evolutions specified by values of α sufficiently far from $\pi/2$ can be smaller than that of evolutions characterized by values of α close to $\pi/2$. This is due to the fact that although Hamiltonians $H_{\text{sub-opt}}(\alpha)$ specified by values α_1 of α sufficiently far from $\pi/2$ yield paths connecting initial and final states that are longer than the ones generated by evolutions characterized by values α_2 of α close to $\pi/2$, they also occupy a larger fraction of the accessible volume than that of evolutions with α close to $\pi/2$. In other words, although $s_1 > s_2$, $(\bar{V}_1/V_{\text{max-1}})^{1/2} \gg (\bar{V}_2/V_{\text{max-2}})^{1/2}$. Thus, being $L_C(\alpha) \stackrel{\text{def}}{=} s \cdot (\bar{V}/V_{\text{max}})^{-1/2}$, $L_C(\alpha_1)$ becomes smaller than $L_C(\alpha_2)$.

α	$\eta_{\text{GE}}(\alpha)$	$\eta_{\text{SE}}(\alpha)$	$\kappa_{\text{AC}}^2(\alpha)$	$C(\alpha)$	$L_C(\alpha)$	$\pi - \alpha$
0	0.7071	0.7071	4	0.3096	2.6735	π
$\frac{1}{16}\pi$	0.7911	0.7204	3.7067	0.3152	2.3996	$\frac{15}{16}\pi$
$\frac{1}{8}\pi$	0.8607	0.7571	2.9781	0.3973	2.3509	$\frac{7}{8}\pi$
$\frac{3}{16}\pi$	0.9128	0.8089	2.1131	0.6259	2.8135	$\frac{13}{16}\pi$
$\frac{1}{4}\pi$	0.9493	0.8660	1.3333	0.6719	2.8888	$\frac{3}{4}\pi$
$\frac{5}{16}\pi$	0.9737	0.9196	0.7298	0.6710	2.8128	$\frac{11}{16}\pi$
$\frac{3}{8}\pi$	0.9890	0.9627	0.3160	0.6706	2.7674	$\frac{5}{8}\pi$
$\frac{7}{16}\pi$	0.9973	0.9904	0.0776	0.6705	2.7439	$\frac{9}{16}\pi$
$\frac{1}{2}\pi$	1	1	0	0.5	2.2214	$\frac{1}{2}\pi$

TABLE II: Numerical estimates of the geodesic efficiency $\eta_{\text{GE}}(\alpha)$, the speed efficiency $\eta_{\text{SE}}(\alpha)$, the curvature coefficient $\kappa_{\text{AC}}^2(\alpha)$, the complexity $C(\alpha)$, and the complexity length scale $L_C(\alpha)$ for $\alpha \in [0, \pi]$. The interval $[0, \pi]$ was partitioned into sixteen sub-intervals of equal size $\pi/16$. Note that all quantities exhibit the same numerical values for the angles α and the corresponding supplementary angles $\pi - \alpha$. This symmetry is expected on physical grounds.

accessible volume in Eq. (39)) parametric volumes of the regions on the Bloch sphere that specify the quantum mechanical evolution from source to target states. Furthermore, we numerically estimated the complexity measure (Table I and Fig. 4) and the complexity length scale (Table I and Fig. 5) for several quantum evolutions specified by Hamiltonians in Eq. (8) for different values of the parameter α that allows to transition from optimal to sub-optimal quantum evolution scenarios. Finally, we compared the behavior of our proposed complexity measures with that of the geodesic efficiency, the speed efficiency, and the curvature coefficient by means of numerical estimates as displayed in Table II. Our work is one of a kind, relating concepts such as complexity, curvature, and efficiency within a single theoretical platform. The main take-home messages are:

- [i] Complexity is more than length. Specifically, quantum evolutions generated by Hamiltonians $H_{\text{sub-opt}}(\alpha)$ in Eq. (8) that connect initial and final states along a shorter path on the Bloch sphere do not need to be necessarily less complex than quantum evolutions connecting the same initial and final states along longer paths. In other words, $\eta_{\text{GE}}(\alpha_1) < \eta_{\text{GE}}(\alpha_2)$ does not generally imply that $C(\alpha_1) > C(\alpha_2)$.
- [ii] Wasting energy resources does not lead automatically to more complex quantum evolutions. Stated otherwise, $\eta_{\text{SE}}(\alpha_1) < \eta_{\text{SE}}(\alpha_2)$ does not generally suggest that $C(\alpha_1) > C(\alpha_2)$.
- [iii] Quantum evolutions yielding longer paths that are sufficiently bent can be less complex than quantum evolutions specified by shorter paths that are less bent. Put differently, $\kappa_{\text{AC}}^2(\alpha_1) > \kappa_{\text{AC}}^2(\alpha_2)$ does not generally signify

that $C(\alpha_1) > C(\alpha_2)$.

- [iv] If one wishes to evolve on the Bloch sphere in the shortest possible time, with maximum speed and no waste of energy resources, the Hamiltonian $H_{\text{opt}} = H_{\text{sub-opt}}(\pi/2)$ remains the best choice, even in terms of our proposed complexity length scale $L_C(\alpha)$. However, if time is not an issue and wasting large amounts of energy resources is tolerated, it is possible to evolve along paths characterized by complexity values smaller than those that specify the shortest possible paths generated by H_{opt} . In other words, it can be $C(\alpha_1) < C(\alpha_2)$ despite the fact that $\eta_{\text{GE}}(\alpha_1) < \eta_{\text{GE}}(\alpha_2)$ and $\eta_{\text{SE}}(\alpha_1) < \eta_{\text{SE}}(\alpha_2)$. This scenario happens when $\bar{V}(\alpha_1)/V_{\text{max}}(\alpha_1) \gg \bar{V}(\alpha_2)/V_{\text{max}}(\alpha_2)$. This set of inequalities is in agreement with the fact that complexity is more than length. This latter statement, in turn, is well-captured by our proposed complexity length scale $L_C(\alpha)$.
- [v] There is no free lunch: If one chooses to move fast and with no waste of energy resources, one must accept some non-minimal level of complexity. If one wishes to minimize the level of complexity, instead, one must give up on speed and on saving energy resources. In any case, our analysis suggests that it is better to pick one of the two extreme scenarios and neglect intermediate cases specified by moderate levels of complexity that do not require so much time and waste of energy resources.

The geometry of quantum state manifolds employed in our work, along with the probabilistic structure underlying the concept of information geometric complexity which is behind our newly proposed quantum complexity measure, allowed us to present in a unifying manner links among quantities such as curvature, efficiency, and complexity measures for quantum evolutions. This is a nontrivial finding in itself. Firstly, focusing on the link between complexity and curvature, we think it would be very helpful carrying out a comparative investigation between our curvature coefficient and the four-index Riemannian curvature introduced in Ref. [64]. Indeed, the four-index Riemannian curvature employed in Ref. [64] was shown to be in a one-to-one correspondence with the fourth cumulant (i.e., the kurtosis) of a cumulant generating function characterizing the Riemannian geometry of the state space of the quantum system being studied. In this context, the Riemann curvature tensor would encode information on the complexity of motion on the manifold of quantum states. Secondly, despite requiring much more study, our quantitative discussion on the connection between lengths and complexity measures defined in terms of volumes originating from probability amplitudes is reminiscent of the rather surprising connection between Krylov's and Nielsen's complexities reported in Ref. [30].

Our work has two obvious restrictions. First, we limited our applications to quantum evolutions governed by stationary Hamiltonians for two-level quantum systems. Second, we neglected any discussion on its applicability to the characterization of the complexity of quantum-mechanical systems in mixed quantum states. In principle, the extension of our work to time-varying Hamiltonian evolutions is conceptually straightforward. However, from a computational standpoint, calculating the expression of probability amplitudes requires precise analytical solutions to the time-dependent Schrödinger equation. This poses significant challenges, even in the context of two-level quantum systems [65–76]. Furthermore, the shift from pure to mixed states presents numerous challenges, both in computational and conceptual aspects. For example, it is established that there exists an infinite variety of distinguishability metrics for mixed quantum states [77]. This variability results in interpretations of significant geometric quantities, such as complexity and volume of quantum states, that are dependent on the chosen metric. Specifically, due to the non-uniqueness of these distinguishability distances, it is essential to comprehend the physical significance of selecting a particular metric, which remains a matter of considerable conceptual and practical importance [78–81]. Given that these above-mentioned complications are beyond the scope of our current work, we will strive to tackle some aspects of these intricacies in forthcoming scientific endeavors.

Regardless of being limited to complexity investigations of geometric style restricted to single-qubit evolutions like the one in Ref. [82], it paves the way to several further investigations. First, we only compared geodesic un wasteful evolutions with nongeodesic wasteful evolutions. However, the spectrum of dynamical possibilities is much richer [83–85]. In particular, it would be interesting to compare (in terms of complexity measures) also geodesic un wasteful paths with geodesic wasteful paths or, alternatively, with nongeodesic un wasteful paths. Second, we can extend the comparative analysis to nonstationary Hamiltonian evolutions specified by physically significant time-dependent magnetic field configurations [71–75]. Third, to investigate the connection between complexity and entanglement, we can expand our approach to d -level quantum systems with $d > 2$ in larger finite-dimensional Hilbert spaces [86–91]. Lastly, we can consider the possibility of offering a comparative analysis of the complexity of quantum evolutions inside the Bloch sphere for quantum systems in mixed quantum states [92, 93].

Regardless of its limitations, we think our work may inspire other scientists to further investigate this research direction. We also believe that our findings can lead to new extensions and applications in the future. We leave a more detailed discussion on these potential advancements for forthcoming scientific efforts.

Acknowledgments

C.C. thanks Emma Clements and Dominic Monaco for helpful comments and discussions, respectively. Furthermore, the authors are grateful to anonymous referees for constructive comments leading to an improved version of the paper. Any opinions, findings and conclusions or recommendations expressed in this material are those of the author(s) and do not necessarily reflect the views of their home Institutions.

-
- [1] L. Susskind, *Computational complexity and black hole horizons*, Fortsch. Phys. **64**, 44 (2016).
- [2] D. Stanford and L. Susskind, *Complexity and shock wave geometries*, Phys. Rev. **D90**, 126007 (2014).
- [3] A. R. Brown, D. A. Roberts, L. Susskind, B. Swingle, and Y. Zhao, *Holographic complexity equals bulk action*, Phys. Rev. Lett. **116**, 191301 (2016).
- [4] A. R. Brown, D. A. Roberts, L. Susskind, B. Swingle, and Y. Zhao, *Complexity, action, and black holes*, Phys. Rev. **D93**, 086006 (2016).
- [5] A. Belin, R. C. Myers, S.-M. Ruan, G. Sarosi, and A. J. Speranza, *Does complexity equal anything?* Phys. Rev. Lett. **128**, 081602 (2022).
- [6] V. B. Bulchandani and S. L. Sondhi, *How smooth is quantum complexity?*, J. High Energ. Phys. **2021**, 230 (2021).
- [7] T. Ali, A. Bhattacharyya, S. Shajidul Haque, E. H. Kim, and N. Moynihan, *Time evolution of complexity: A critique of three methods*, J. High Energ. Phys. **2019**, 87 (2019).
- [8] T. Ali, A. Bhattacharyya, S. Shajidul Haque, E. H. Kim, N. Moynihan, and J. Murugan, *Chaos and complexity in quantum mechanics*, Phys. Rev. **D101**, 026021 (2020).
- [9] V. Balasubramanian, M. DeCross, A. Kar, and O. Parrikar, *Quantum complexity of time evolution with chaotic Hamiltonians*, J. High Energ. Phys. **2020**, 134 (2020).
- [10] C. Gomez, *Complexity and time*, Phys. Rev. **D101**, 065016 (2020).
- [11] S. Chapman, M. P. Heller, H. Marrochio, and F. Pastawski, *Toward a definition of complexity for quantum field theory states*, Phys. Rev. Lett. **120**, 121602 (2018).
- [12] J. Iaconis, *Quantum state complexity in computationally tractable quantum circuits*, PRX Quantum **2**, 010329 (2021).
- [13] M. A. Nielsen and I. L. Chuang, *Quantum Computation and Quantum Information*, Cambridge University Press (2000).
- [14] F. G. S. L. Brandao, W. Chemissany, N. Hunter-Jones, R. Kueng, and J. Preskill, *Models of quantum complexity growth*, PRX Quantum **2**, 030316 (2021).
- [15] D. E. Parker, X. Cao, A. Avdoshkin, T. Scaffidi, and E. Altman, *A universal operator growth hypothesis*, Phys. Rev. **X9**, 041017 (2019).
- [16] K. Adhikari, S. Choudhury, and A. Roy, *Krylov complexity in quantum field theory*, Nucl. Phys. **B993**, 116263 (2023).
- [17] C. Liu, H. Tang, and H. Zhai, *Krylov complexity in open quantum systems*, Phys. Rev. Research **5**, 033085 (2023).
- [18] P. Caputa, J. M. Magan, and D. Patramanis, *Geometry of Krylov complexity*, Phys. Rev. Research **4**, 013041 (2022).
- [19] L. Lofgren, *Complexity of descriptions of systems: A foundational study*, Int. J. General Systems **3**, 197 (1977).
- [20] E. Olbrich, N. Bertschinger, N. Ay, and J. Jost, *How should complexity scale with system size?*, Eur. Phys. J. **B63**, 407 (2008).
- [21] V. Balasubramanian, P. Caputa, J. M. Magan, and Q. Wu, *Quantum chaos and the complexity of spread of states*, Phys. Rev. **D106**, 046007 (2022).
- [22] A. N. Kolmogorov, *Three approaches to the quantitative definition of information*, Int. J. Computer Mathematics **2**, 157 (1968).
- [23] J. Rissanen, *Modeling by the shortest data description*, Automatica **14**, 465 (1978).
- [24] J. Rissanen, *Stochastic complexity and modeling*, Ann. Stat. **14**, 1080 (1986).
- [25] M. A. Nielsen, *A geometric approach to quantum circuit lower bounds*, Quant. Inf. Comput. **6**, 213 (2006).
- [26] M. A. Nielsen, M. R. Dowling, M. Gu, and A. M. Doherty, *Quantum computation as geometry*, Science **311**, 1133 (2006).
- [27] M. R. Dowling and M. A. Nielsen, *The geometry of quantum computation*, Quant. Inf. Comput. **8**, 861 (2008).
- [28] B. Craps, M. De Clerck, O. Evnin, P. Hacker, and M. Pavlov, *Bounds on quantum evolution complexity via lattice cryptography*, SciPost Phys. **13**, 090 (2022).
- [29] B. Craps, M. De Clerck, O. Evnin, and P. Hacker, *Integrability and complexity in quantum spin chains*, SciPost Phys. **16**, 041 (2024).
- [30] B. Craps, O. Evnin, and G. Pascuzzi, *A relation between Krylov and Nielsen complexity*, Phys. Rev. Lett. **132**, 160402 (2024).
- [31] C. Cafaro and P. M. Alsing, *Complexity of pure and mixed qubit geodesic paths on curved manifolds*, Phys. Rev. **D106**, 096004 (2022).
- [32] S. L. Braunstein and C. M. Caves, *Statistical distance and the geometry of quantum states*, Phys. Rev. Lett. **72**, 3439 (1994).
- [33] E. Sjöqvist, *Geometry along evolution of mixed quantum states*, Phys. Rev. Research **2**, 013344 (2020).
- [34] P. M. Alsing, C. Cafaro, O. Luongo, C. Lupo, S. Mancini, and H. Quevedo, *Comparing metrics for mixed quantum states: Sjöqvist and Bures*, Phys. Rev. **A107**, 052411 (2023).
- [35] W. K. Wootters, *Statistical distance and Hilbert space*, Phys. Rev. **D23**, 357 (1981).

- [36] J. P. Provost and G. Vallee, *Riemannian structure on manifolds of quantum states*, Commun. Math. Phys. **76**, 289 (1980).
- [37] C. Cafaro and P. M. Alsing, *Qubit geodesics on the Bloch sphere from optimal-speed Hamiltonian evolutions*, Class. Quantum Grav. **40**, 115005 (2023).
- [38] J. Anandan and Y. Aharonov, *Geometry of quantum evolution*, Phys. Rev. Lett. **65**, 1697 (1990).
- [39] C. Cafaro, S. Ray, and P. M. Alsing, *Geometric aspects of analog quantum search evolutions*, Phys. Rev. **A102**, 052607 (2020).
- [40] R. Uzdin, U. Günther, S. Rahav, and N. Moiseyev, *Time-dependent Hamiltonians with 100% evolution speed efficiency*, J. Phys. A: Math. Theor. **45**, 415304 (2012).
- [41] P. M. Alsing and C. Cafaro, *From the classical Frenet–Serret apparatus to the curvature and torsion of quantum-mechanical evolutions. Part I. Stationary Hamiltonians*, Int. J. Geom. Methods Mod. Phys. **21**, 2450152 (2024).
- [42] P. M. Alsing and C. Cafaro, *From the classical Frenet–Serret apparatus to the curvature and torsion of quantum-mechanical evolutions. Part II. Nonstationary Hamiltonians*, Int. J. Geom. Methods Mod. Phys. **21**, 2450151 (2024).
- [43] C. Cafaro and S. A. Ali, *Jacobi fields on statistical manifolds of negative curvature*, Physica **D234**, 70 (2007).
- [44] C. Cafaro, *The Information Geometry of Chaos*, Ph. D. Thesis, University at Albany-SUNY, USA (2008).
- [45] S. A. Ali and C. Cafaro, *Theoretical investigations of an information geometric approach to complexity*, Rev. Math. Phys. **29**, 1730002 (2017).
- [46] D. Felice, C. Cafaro, and S. Mancini, *Information geometric methods for complexity*, Chaos **28**, 032101 (2018).
- [47] D. C. Brody and D. W. Hook, *On optimum Hamiltonians for state transformations*, J. Phys. A: Math. Gen. **39**, L167 (2006).
- [48] D. C. Brody and D. W. Hook, *On optimum Hamiltonians for state transformation*, J. Phys. A: Math. Theor. **40**, 10949 (2007).
- [49] C. M. Bender, D. C. Brody, H. F. Jones, and B. K. Meister, *Faster than Hermitian quantum mechanics*, Phys. Rev. Lett. **98**, 040403 (2007).
- [50] C. M. Bender and D. C. Brody, *Optimal time evolution for Hermitian and non-Hermitian Hamiltonians*, Lecture Notes in Physics **789**, 341 (2009).
- [51] A. Mostafazadeh, *Hamiltonians generating optimal-speed evolutions*, Phys. Rev. **A79**, 014101 (2009).
- [52] L. Rossetti, C. Cafaro, N. Bahreyni, *Constructions of optimal-speed quantum evolutions: A comparative study*, Physica Scripta **99**, 095121 (2024).
- [53] L. Rossetti, C. Cafaro, and P. M. Alsing, *Quantifying deviations from shortest geodesic paths together with waste of energy resources for quantum evolutions in projective Hilbert space*, arXiv:quant-ph/2408.14230 (2024).
- [54] S. A. Ali, C. Cafaro, S. Gassner, and A. Giffin, *An information geometric perspective on the complexity of macroscopic predictions arising from incomplete information*, Adv. Math. Phys., Volume 2018, Article ID 2048521 (2018).
- [55] C. Cafaro and S. A. Ali, *Information geometric measures of complexity with applications to classical and quantum physical settings*, Foundations **1**, 45 (2021).
- [56] S. A. Ali, C. Cafaro, D.-H. Kim, and S. Mancini, *The effect of microscopic correlations on the information geometric complexity of Gaussian statistical models*, Physica **A389**, 3117 (2010).
- [57] I. S. Gradshteyn and I. M. Ryzhik, *Tables of Integrals, Series, and Products*, Academic Press (2000).
- [58] B. Beizer, *Software System Testing and Quality Assurance*, Van Nostrand Reinhold Company Publisher, New York (1984).
- [59] G. K. Gill and C. F. Kremerer, *Cyclomatic complexity density and software maintenance*, IEEE Trans. Software Engineering **17**, 1284 (1991).
- [60] T. Andersson, K. Enholm, and A. Torn, *Length-independent measure of software complexity*, Transactions on Information and Communications Technologies **8**, 349 (1994).
- [61] J. T. Bonner, *The size-complexity rule*, Evolution **58**, 1883 (2004).
- [62] J. Myung, V. Balasubramanian, and M. A. Pitt, *Counting probability distributions: Differential geometry and model selection*, PNAS **97**, 11170 (2000).
- [63] L. Diosi, G. Forgacs, B. Lukacs, and H. L. Frisch, *Metricization of thermodynamic-state space and the renormalization group*, Phys. Rev. **A29**, 3343 (1984).
- [64] B. Hetenyi and P. Levay, *Fluctuations, uncertainty relations, and the geometry of quantum state manifolds*, Phys. Rev. **A108**, 032218 (2023).
- [65] L. Landau, *A theory of energy transfer. II*, Phys. Z. Sowjet **2**, 46 (1932).
- [66] C. Zener, *Non-adiabatic crossing of energy levels*, Proc. R. Soc. **A137**, 696 (1932).
- [67] I. I. Rabi, *Space quantization in a gyrating magnetic field*, Phys. Rev. **51**, 652 (1937).
- [68] I. I. Rabi, N. F. Ramsey, and J. Schwinger, *Use of rotating coordinates in magnetic resonance problems*, Rev. Mod. Phys. **26**, 167 (1954).
- [69] E. Barnes and S. Das Sarma, *Analytically solvable driven time-dependent two-level quantum systems*, Phys. Rev. Lett. **109**, 060401 (2012).
- [70] E. Barnes, *Analytically solvable two-level quantum systems and Landau-Zener interferometry*, Phys. Rev. **A88**, 013818 (2013).
- [71] A. Messina and H. Nakazato, *Analytically solvable Hamiltonians for quantum two-level systems and their dynamics*, J. Phys. A: Math and Theor. **47**, 44302 (2014).
- [72] R. Grimauco, A. S. Magalhaes de Castro, H. Nakazato, and A. Messina, *Classes of exactly solvable generalized semi-classical Rabi systems*, Annalen der Physik **530**, 1800198 (2018).
- [73] C. Cafaro and P. M. Alsing, *Continuous-time quantum search and time-dependent two-level quantum systems*, Int. J. Quantum Information **17**, 1950025 (2019).

- [74] L. O. Castanos, *Simple, analytic solutions of the semiclassical Rabi model*, Optics Communications **430**, 176 (2019).
- [75] A. S. Magalhaes de Castro, R. Grimaudo, D. Valenti, A. Migliore, H. Nakazato, and A. Messina, *Analytically solvable Hamiltonian in invariant subspaces*, Eur. Phys. J. Plus **138**, 766 (2023).
- [76] E. R. Loubenets and C. Kading, *Specifying the unitary evolution of a qudit for a general nonstationary Hamiltonian via the generalized Gell-Mann representation*, Entropy **22**, 521 (2020).
- [77] I. Bengtsson and K. Życzkowski, *Geometry of Quantum States*, Cambridge University Press (2006).
- [78] H. Silva, B. Mera, and N. Paunkovic, *Interferometric geometry from symmetry-broken Uhlmann gauge group with applications to topological phase transitions*, Phys. Rev. **B103**, 085127 (2021).
- [79] B. Mera, N. Paunkovic, S. T. Amin, and V. R. Vieira, *Information geometry of quantum critical submanifolds: Relevant, marginal, and irrelevant operators*, Phys. Rev. **B106**, 155101 (2022).
- [80] P. M. Alsing, C. Cafaro, D. Felice, and O. Luongo, *Geometric aspects of mixed quantum states inside the Bloch sphere*, Quantum Reports **6**, 90 (2024).
- [81] X.-Y. Hou, Z. Zhou, X. Wang, H. Guo, and C.-C. Chien, *Local geometry and quantum geometric tensor of mixed states*, Phys. Rev. **B110**, 035144 (2024).
- [82] A. R. Brown and L. Susskind, *Complexity geometry of a single qubit*, Phys. Rev. **D100**, 046020 (2019).
- [83] F. Campaioli, F. A. Pollock, and K. Modi, *Tight, robust, and feasible quantum speed limits for open dynamics*, Quantum **3**, 168 (2019).
- [84] F. Campaioli, W. Sloan, K. Modi, and F. A. Pollock, *Algorithm for solving unconstrained unitary quantum brachistochrone problems*, Phys. Rev. **A100**, 062328 (2019).
- [85] J. Xu et al., *Balancing the quantum speed limit and instantaneous energy cost in adiabatic quantum evolution*, Chinese Phys. Lett. **41**, 040202 (2024).
- [86] L. Jakobczyk and M. Siennicki, *Geometry of Bloch vectors in two-qubit system*, Phys. Lett. **A286**, 383 (2001).
- [87] G. Kimura, *The Bloch vector for N-level systems*, Phys. Lett. **A314**, 339 (2003).
- [88] R. A. Bertlmann and P. Krammer, *Bloch vectors for qudits*, J. Phys. A: Math. Theor. **41**, 235303 (2008).
- [89] P. Kurzynski, *Multi-Bloch vector representation of the qutrit*, Quantum Inf. Comp. **11**, 361 (2011).
- [90] J. Xie et al., *Observing geometry of quantum states in a three-level system*, Phys. Rev. Lett. **125**, 150401 (2020).
- [91] C. Eltschka, M. Huber, S. Morelli, and J. Siewert, *The shape of higher-dimensional state space: Bloch-ball analog for a qutrit*, Quantum **5**, 485 (2021).
- [92] N. Hornedal, D. Allan, and O. Sonnerborn, *Extensions of the Mandelstam-Tamm quantum speed limit to systems in mixed states*, New J. Phys. **24**, 055004 (2022).
- [93] A. Naderzadeh-ostad and S. J. Akhtarshenas, *Optimal quantum speed for mixed states*, J. Phys. A: Math. Theor. **57**, 075301 (2024).

Appendix A: Complexity symmetries

In this Appendix, we demonstrate that for the class of Hamiltonian evolutions considered in Eq. (8), the accessed volume $\bar{V}(\alpha, \omega)$ and the accessible volume $V_{\max}(\alpha, \omega)$ do not depend on $\omega \stackrel{\text{def}}{=} E/\hbar$. Furthermore, we show that $\bar{V}(\alpha) = \bar{V}(\pi - \alpha)$ and $V_{\max}(\alpha) = V_{\max}(\pi - \alpha)$. Thus, the complexity $C(\alpha)$ and the complexity length scale $L_C(\alpha)$ assume identical values for supplementary angles α and $\pi - \alpha$ for any choice of the value for the frequency ω (or, alternatively, for any finite energy value E).

To show that $\bar{V}(\alpha, \omega)$ does not depend on ω , we note that the time-dependent volume $V(t; \alpha, \omega)$ in Eq. (52) is such that $V(t; \alpha, \omega) = V(\omega t; \alpha)$. Therefore, $\bar{V}(\alpha, \omega)$ can be recast as

$$\bar{V}(\alpha, \omega) = \frac{1}{t_*} \int_0^{t_*} V(\omega t; \alpha) dt, \quad (\text{A1})$$

where $t_* \stackrel{\text{def}}{=} f(\alpha, \theta_{AB})/\omega$ and $f(\alpha, \theta_{AB}) \stackrel{\text{def}}{=} \omega t_{AB}(\alpha)$ with $t_{AB}(\alpha)$ in Eq. (11). Performing a change of the integration variable t in Eq. (A1) and setting $\tau \stackrel{\text{def}}{=} \omega t$, $\bar{V}(\alpha, \omega)$ in Eq. (A1) reduces to

$$\bar{V}(\alpha, \omega) = \frac{1}{f(\alpha, \theta_{AB})} \int_0^{f(\alpha, \theta_{AB})} V(\tau; \alpha) d\tau \stackrel{\text{def}}{=} \bar{V}(\alpha), \quad (\text{A2})$$

that is, $\bar{V}(\alpha, \omega) = \bar{V}(\alpha)$. Clearly, for different values of θ_{AB} , we generally get different values for $\bar{V}(\alpha)$. In our applications, θ_{AB} equals $\pi/2$. To understand that $V_{\max}(\alpha, \omega)$ does not depend on ω , it is sufficient to note that optimizing $\theta(t; \alpha, \omega)$ (or, analogously, $\varphi(t; \alpha, \omega)$) over the time interval $0 \leq t \leq t_* \stackrel{\text{def}}{=} f(\alpha, \theta_{AB})/\omega$ is equivalent to optimizing $\theta(\omega t; \alpha)$ over $0 \leq \omega t \leq f(\alpha, \theta_{AB})$ (given the temporal behaviors of $\theta(t; \alpha, \omega)$ and $\varphi(t; \alpha, \omega)$ in Eqs. (50) and (51), respectively). Therefore, putting $\tau \stackrel{\text{def}}{=} \omega t$, the optimization of $\theta(t; \alpha, \omega)$ over $0 \leq t \leq f(\alpha, \theta_{AB})/\omega$ is the same as the optimization of $\theta(\tau; \alpha)$ over $0 \leq \tau \leq f(\alpha, \theta_{AB})$. Therefore, we conclude that $V_{\max}(\alpha, \omega)$ is independent from ω . To be more explicit, we remark that $\theta(t; \alpha, \omega_1)$ and $\theta(t; \alpha, \omega_2)$ with $\omega_1 \neq \omega_2$ assume the same minimum and maximum values. However, they occur at different times $t_1 \stackrel{\text{def}}{=} f(\alpha, \theta_{AB})/\omega_1$ and $t_2 \stackrel{\text{def}}{=} f(\alpha, \theta_{AB})/\omega_2$, respectively. Furthermore, to understand the reason why $\bar{V}(\alpha) = \bar{V}(\pi - \alpha)$, it suffices observing that $f(\alpha, \theta_{AB})$ in Eq. (A2) equals $\omega t_{AB}(\alpha)$ with $t_{AB}(\alpha)$ in Eq. (11) and, thus, is such that $f(\alpha, \theta_{AB}) = f(\pi - \alpha, \theta_{AB})$. This latter relation, in turn, is a consequence of the fact that $t_{AB}(\alpha) = t_{AB}(\pi - \alpha)$ (given that $\sin(\pi - \alpha) = \sin(\alpha)$, $\cos^2(\pi - \alpha) = \cos^2(\alpha)$, and $\sin^2(\pi - \alpha) = \sin^2(\alpha)$). Finally, to justify why $V_{\max}(\alpha) = V_{\max}(\pi - \alpha)$, we begin by noting that $\theta_{\min}(\alpha) = \pi/2$ and $\theta_{\max}(\alpha) = \xi$ for some $\xi > \pi/2$. Then, geometric arguments require $\theta_{\max}(\alpha) - \theta_{\min}(\alpha) = \theta_{\max}(\pi - \alpha) - \theta_{\min}(\pi - \alpha)$ and $\theta_{\max}(\pi - \alpha) = \theta_{\min}(\alpha) = \pi/2$. Therefore, we get $\theta_{\min}(\pi - \alpha) = \pi - \xi$. Observe that for both the α and $\pi - \alpha$ angles, the azimuthal angle belongs to the interval $[0, \pi/2]$ with $\varphi_{\min} = 0$ and $\varphi_{\max} = \pi/2$. Therefore, given these lower and upper bounds for the polar angles, $V_{\max}(\alpha) = V_{\max}(\pi - \alpha)$ follows from the fact that

$$\int_{\frac{\pi}{2}}^{\xi} \sin(\theta) d\theta = \int_{\pi - \xi}^{\frac{\pi}{2}} \sin(\theta) d\theta. \quad (\text{A3})$$

With the presentation of the identity in Eq. (A3), we end our discussion on some essential symmetry properties exhibited by the complexity $C(\alpha) \stackrel{\text{def}}{=} [V_{\max}(\alpha) - \bar{V}(\alpha)]/V_{\max}(\alpha)$ and the complexity length scale $L_C(\alpha) \stackrel{\text{def}}{=} s(\alpha)/\sqrt{1 - C(\alpha)}$.

Appendix B: Complexity calculations

In this Appendix, we show some technical details on how to calculate the complexity $C(\alpha)$ in Eq. (29) and the complexity length scale $L_C(\alpha)$ in Eq. (44) for two supplementary angles, $\alpha_1 \stackrel{\text{def}}{=} (1/16)\pi$ and $\alpha_2 \stackrel{\text{def}}{=} \pi - \alpha_1 = (15/16)\pi$. A similar calculation scheme applies to any other pair of supplementary angles α and $\pi - \alpha$, with $0 \leq \alpha \leq \pi$. Clearly, the essential quantities needed to arrive at the estimates of $C(\alpha)$ and $L_C(\alpha)$ are the accessed volume $\bar{V}(\alpha, \omega)$ in Eq. (34), the accessible volume $V_{\max}(\alpha, \omega)$ in Eq. (39), and the path length $s(\alpha)$ in Eq. (12). We recall that we set in what follows $\hbar = 1$ and $\omega \stackrel{\text{def}}{=} E/\hbar = 1$. Although we do not use physical units in an explicit fashion, assume that the usual MKSA unit system is employed here.

1. Case: $\alpha_1 = \pi/16$

For $\alpha_1 = \pi/16$, the time-dependent volume $V(t)$ in Eq. (52) becomes

$$V(t) = \frac{1}{4} |\varphi(t) \cos[\theta(t)]|. \quad (\text{B1})$$

The polar and azimuthal angles in Eq. (B1) are given by,

$$\theta(t) \stackrel{\text{def}}{=} 2 \arctan \left(\sqrt{\frac{\frac{1}{2} - \frac{\sin(\frac{\pi}{8})}{2\sqrt{2}} \sin^2(t) + \frac{\cos(\frac{\pi}{16})}{2\sqrt{2}} \sin(2t)}{\frac{1}{2} + \frac{\sin(\frac{\pi}{8})}{2\sqrt{2}} \sin^2(t) - \frac{\cos(\frac{\pi}{16})}{2\sqrt{2}} \sin(2t)}} \right), \quad (\text{B2})$$

and,

$$\varphi(t) \stackrel{\text{def}}{=} \begin{cases} \varphi_1(t) \stackrel{\text{def}}{=} \arctan \left(\frac{\frac{\sin(\frac{\pi}{16}) \sin(t)}{\sqrt{2}} - \frac{\cos(\frac{\pi}{16}) \sin(t)}{2}}{\frac{\cos(\frac{\pi}{16}) \sin(t)}{2} + \frac{\cos(t)}{\sqrt{2}}} \right) - \arctan \left(\frac{\frac{\cos(\frac{\pi}{16}) \sin(t)}{2} + \frac{\sin(\frac{\pi}{16}) \sin(t)}{\sqrt{2}}}{\frac{\cos(\frac{\pi}{16}) \sin(t)}{2} - \frac{\cos(t)}{\sqrt{2}}} \right), & \text{for } 0 \leq t \leq t_1 \\ \varphi_2(t) \stackrel{\text{def}}{=} \arctan \left(\frac{\frac{\sin(\frac{\pi}{16}) \sin(t)}{\sqrt{2}} - \frac{\cos(\frac{\pi}{16}) \sin(t)}{2}}{\frac{\cos(\frac{\pi}{16}) \sin(t)}{2} + \frac{\cos(t)}{\sqrt{2}}} \right) - \arctan \left(\frac{\frac{\cos(\frac{\pi}{16}) \sin(t)}{2} + \frac{\sin(\frac{\pi}{16}) \sin(t)}{\sqrt{2}}}{\frac{\cos(\frac{\pi}{16}) \sin(t)}{2} - \frac{\cos(t)}{\sqrt{2}}} \right) + \pi, & \text{for } t_1 \leq t \leq t_2 \end{cases}, \quad (\text{B3})$$

respectively, with $t_1 \stackrel{\text{def}}{=} \arctan \{ \sqrt{2} / [\cos(\frac{\pi}{16})] \} \simeq 0.9644$ and $t_2 \simeq 1.3781$ being the time needed to arrive from the initial state $|A\rangle$ to the final state $|B\rangle$. Using Eqs. (B1), (B2), and (B3), the accessed volume \bar{V} becomes

$$\bar{V} = \frac{1}{t_1} \int_0^{t_1} \frac{1}{4} |\varphi_1(t) \cos[\theta(t)]| dt + \frac{1}{t_2 - t_1} \int_{t_1}^{t_2} \frac{1}{4} |\varphi_2(t) \cos[\theta(t)]| dt. \quad (\text{B4})$$

From a numerical integration of the right-hand-side in Eq. (B4), we get $\bar{V} = 6.5385 \times 10^{-2} + 8.8238 \times 10^{-2} \simeq 0.1536$. Next, to get an estimate of V_{\max} , we need to find θ_{\min} , θ_{\max} , φ_{\min} , and φ_{\max} . Inspecting Eqs. (B2) and (B3), we obtain $\theta_{\min} = \theta(0) = \pi/2 \simeq 1.5708$, $\theta_{\max} = \theta((t_B - t_A)/2) = \theta(1.3781/2) \simeq 2.1789$, $\varphi_{\min} = \varphi(0) = 0$, and $\varphi_{\max} = \varphi(t_B - t_A) = \varphi(1.3781) = \pi/2 \simeq 1.5708$. Therefore, V_{\max} is equal to

$$V_{\max} = \frac{1}{4} \left(\int_{\theta_{\min}}^{\theta_{\max}} \sin(\theta) d\theta \right) \left(\int_{\varphi_{\min}}^{\varphi_{\max}} d\varphi \right), \quad (\text{B5})$$

that is, $V_{\max} \simeq 0.2243$. From Table III, we see that $s = 1.9857$ for $\alpha_1 = \pi/16$. Therefore, using the numerical estimates of \bar{V} , V_{\max} , and s , we finally arrive at $C \simeq 0.3152$ and $L_C \simeq 2.3996$. These are the values that appear in Tables I and II.

2. Case: $\alpha_2 = (15/16)\pi$

For $\alpha_2 = (15/16)\pi$, the time-dependent volume $V(t)$ in Eq. (52) become

$$V(t) = \frac{1}{4} |\varphi(t) \cos[\theta(t)]|. \quad (\text{B6})$$

The polar and azimuthal angles in Eq. (B1) are given by,

$$\theta(t) \stackrel{\text{def}}{=} 2 \arctan \left(\sqrt{\frac{\frac{1}{2} - \frac{\sin(\frac{15}{8}\pi)}{2\sqrt{2}} \sin^2(t) + \frac{\cos(\frac{15}{16}\pi)}{2\sqrt{2}} \sin(2t)}{\frac{1}{2} + \frac{\sin(\frac{15}{8}\pi)}{2\sqrt{2}} \sin^2(t) - \frac{\cos(\frac{15}{16}\pi)}{2\sqrt{2}} \sin(2t)}} \right), \quad (\text{B7})$$

and,

$$\varphi(t) \stackrel{\text{def}}{=} \begin{cases} \varphi_1(t) \stackrel{\text{def}}{=} \arctan \left(\frac{\frac{\sin(\frac{15}{16}\pi) \sin(t)}{\sqrt{2}} - \frac{\cos(\frac{15}{16}\pi) \sin(t)}{2}}{\frac{\cos(\frac{15}{16}\pi) \sin(t)}{2} + \frac{\cos(t)}{\sqrt{2}}} \right) - \arctan \left(\frac{\frac{\cos(\frac{15}{16}\pi) \sin(t)}{2} + \frac{\sin(\frac{15}{16}\pi) \sin(t)}{\sqrt{2}}}{\frac{\cos(\frac{15}{16}\pi) \sin(t)}{2} - \frac{\cos(t)}{\sqrt{2}}} \right), & \text{for } 0 \leq t \leq t_1 \\ \varphi_2(t) \stackrel{\text{def}}{=} \arctan \left(\frac{\frac{\sin(\frac{15}{16}\pi) \sin(t)}{\sqrt{2}} - \frac{\cos(\frac{15}{16}\pi) \sin(t)}{2}}{\frac{\cos(\frac{15}{16}\pi) \sin(t)}{2} + \frac{\cos(t)}{\sqrt{2}}} \right) - \arctan \left(\frac{\frac{\cos(\frac{15}{16}\pi) \sin(t)}{2} + \frac{\sin(\frac{15}{16}\pi) \sin(t)}{\sqrt{2}}}{\frac{\cos(\frac{15}{16}\pi) \sin(t)}{2} - \frac{\cos(t)}{\sqrt{2}}} \right) + \pi, & \text{for } t_1 \leq t \leq t_2 \end{cases}, \quad (\text{B8})$$

α	$t(\alpha)$	$s(\alpha)$	$\pi - \alpha$
0	1.5708	2.2214	π
$\frac{1}{16}\pi$	1.3781	1.9857	$\frac{15}{16}\pi$
$\frac{1}{8}\pi$	1.2053	1.8251	$\frac{7}{8}\pi$
$\frac{3}{16}\pi$	1.0637	1.7208	$\frac{13}{16}\pi$
$\frac{1}{4}\pi$	0.9553	1.6547	$\frac{3}{4}\pi$
$\frac{5}{16}\pi$	0.8772	1.6133	$\frac{11}{16}\pi$
$\frac{3}{8}\pi$	0.8249	1.5883	$\frac{5}{8}\pi$
$\frac{7}{16}\pi$	0.7951	1.5750	$\frac{9}{16}\pi$
$\frac{1}{2}\pi$	0.7854	1.5708	$\frac{1}{2}\pi$

TABLE III: Numerical estimates for the evolution time $t(\alpha)$ and the length of the path $s(\alpha)$, with $0 \leq \alpha \leq \pi$. The interval $[0, \pi]$ was partitioned into sixteen sub-intervals of equal size $\pi/16$. We set $\hbar = 1$ and $\omega = 1$ in the calculations.

respectively, with $t_1 \stackrel{\text{def}}{=} \arctan \{ \sqrt{2} / [\cos(\frac{\pi}{16})] \} \simeq 0.9644$ and $t_2 \simeq 1.3781$ being the time needed to arrive from the initial state $|A\rangle$ to the final state $|B\rangle$. To find t_1 , we used the fact that $\cos(\pi/16) = -\cos[(15/16)\pi]$. Using Eqs. (B6), (B7), and (B8), the accessed volume \bar{V} reduces to

$$\bar{V} = \frac{1}{t_1} \int_0^{t_1} \frac{1}{4} |\varphi_1(t) \cos[\theta(t)]| dt + \frac{1}{t_2 - t_1} \int_{t_1}^{t_2} \frac{1}{4} |\varphi_2(t) \cos[\theta(t)]| dt. \quad (\text{B9})$$

From a numerical integration of the right-hand-side in Eq. (B9), we get $\bar{V} = 6.5385 \times 10^{-2} + 8.8238 \times 10^{-2} \simeq 0.1536$. Next, to get an estimate of V_{\max} , we need to find θ_{\min} , θ_{\max} , φ_{\min} , and φ_{\max} . Inspecting Eqs. (B7) and (B8), we obtain $\theta_{\min} = \theta((t_B - t_A)/2) = \theta(1.3781/2) \simeq 0.9627$, $\theta_{\max} = \theta(0) = \pi/2 \simeq 1.5708$, $\varphi_{\min} = \varphi(0) = 0$, and $\varphi_{\max} = \varphi(t_B - t_A) = \varphi(1.3781) = \pi/2 \simeq 1.5708$. Therefore, V_{\max} equals

$$V_{\max} = \frac{1}{4} \left(\int_{\theta_{\min}}^{\theta_{\max}} \sin(\theta) d\theta \right) \left(\int_{\varphi_{\min}}^{\varphi_{\max}} d\varphi \right), \quad (\text{B10})$$

that is, $V_{\max} \simeq 0.2243$. From Table III, we see that $s = 1.9857$ for $\alpha_2 = (15/16)\pi$. Therefore, using the numerical estimates of \bar{V} , V_{\max} , and s , we finally arrive at $C \simeq 0.3152$ and $L_C \simeq 2.3996$. These are the values that are displayed in Tables I and II.